JOURNAL OF GEOPHYSICAL RESEARCH, VOL. 108, NO. D3, 4097, doi:10.1029/2002JD002622, 2003

Global and regional decreases in tropospheric oxidants from photochemical effects of aerosols

Randall V. Martin,[1] Daniel J. Jacob, and Robert M. Yantosca

Division of Engineering and Applied Sciences, and Department of Earth and Planetary Sciences, Harvard University, Cambridge, Massachusetts, USA

Mian Chin[2] and Paul Ginoux[2]

School of Earth and Atmospheric Sciences, Georgia Institute of Technology, Atlanta, Georgia, USA

Received 5 June 2002; revised 28 August 2002; accepted 28 August 2002; published 5 February 2003.

[1] We evaluate the sensitivity of tropospheric OH, O_3, and O_3 precursors to photochemical effects of aerosols not usually included in global models: (1) aerosol scattering and absorption of ultraviolet radiation and (2) reactive uptake of HO_2, NO_2, and NO_3. Our approach is to couple a global 3-D model of tropospheric chemistry (GEOS-CHEM) with aerosol fields from a global 3-D aerosol model (GOCART). Reactive uptake by aerosols is computed using reaction probabilities from a recent review ($\gamma_{HO2} = 0.2$, $\gamma_{NO2} = 10^{-4}$, $\gamma_{NO3} = 10^{-3}$). Aerosols decrease the $O_3 \rightarrow O(^1D)$ photolysis frequency by 5–20% at the surface throughout the Northern Hemisphere (largely due to mineral dust) and by a factor of 2 in biomass burning regions (largely due to black carbon). Aerosol uptake of HO_2 accounts for 10–40% of total HO_x radical ($\equiv$ OH + peroxy) loss in the boundary layer over polluted continental regions (largely due to sulfate and organic carbon) and for more than 70% over tropical biomass burning regions (largely due to organic carbon). Uptake of NO_2 and NO_3 accounts for 10–20% of total HNO_3 production over biomass burning regions and less elsewhere. Annual mean OH concentrations decrease by 9% globally and by 5–35% in the boundary layer over the Northern Hemisphere. Simulated CO increases by 5–15 ppbv in the remote Northern Hemisphere, improving agreement with observations. Simulated boundary layer O_3 decreases by 15–45 ppbv over India during the biomass burning season in March and by 5–9 ppbv over northern Europe in August, again improving comparison with observations. We find that particulate matter controls would increase surface O_3 over Europe and other industrial regions. *INDEX TERMS:* 0305 Atmospheric Composition and Structure: Aerosols and particles (0345, 4801); 0345 Atmospheric Composition and Structure: Pollution—urban and regional (0305); 0360 Atmospheric Composition and Structure: Transmission and scattering of radiation; 0365 Atmospheric Composition and Structure: Troposphere—composition and chemistry; *KEYWORDS:* aerosols, ozone, heterogeneous chemistry, radiation, reactive uptake, OH

Citation: Martin, R. V., D. J. Jacob, R. M. Yantosca, M. Chin, and P. Ginoux, Global and regional decreases in tropospheric oxidants from photochemical effects of aerosols, *J. Geophys. Res.*, *108*(D3), 4097, doi:10.1029/2002JD002622, 2003.

1. Introduction

[2] Understanding the radiative and heterogeneous chemical effects of aerosols on OH and O_3, the main tropospheric oxidants, is a major issue for models of the oxidizing power of the atmosphere, radiative forcing, and surface air quality. The importance of N_2O_5 hydrolysis in aerosols is well established [*Heikes and Thompson*, 1983; *Dentener and Crutzen*, 1993; *Tie et al.*, 2001; *Liao et al.*, 2003] and is included in all current-generation global models of tropospheric chemistry. Model calculations by *Dentener and Crutzen* [1993] indicate that this reaction reduces global tropospheric O_3 and OH by 9%. Other aerosol effects have received far less study and are the focus of this paper.

[3] Scattering and absorption of ultraviolet (UV) radiation by aerosols modifies photolysis rates [*He and Carmichael*, 1999; *Liao et al.*, 1999]. Reactive heterogeneous uptake of HO_2, NO_2, and NO_3 by aerosols may be important as well [*Jacob*, 2000]. Including these photochemical effects of aerosols in global models could help resolve some long-standing discrepancies with measurements, such as the underestimate of the CO background in the Northern Hemisphere [*Hauglustaine et al.*, 1998; *Lawrence et al.*, 1999; *Bergamaschi et al.*, 2000, 2001; *Bey et al.*, 2001a] and the

[1] Now at Harvard-Smithsonian Center for Astrophysics, Cambridge, Massachusetts, USA.

[2] Also at NASA Goddard Space Flight Center, Greenbelt, Maryland, USA.

0148-0227/03/2002JD002622$09.00

overestimate of O_3 over India [*Lal and Lawrence*, 2001; *Martin et al.*, 2002b].

[4] Recent development of global simulations and observational databases for the major aerosol types (sulfate, black carbon, organic carbon, sea salt, and mineral dust) [*Tegen et al.*, 1997; *Takemura et al.*, 2000; *Ghan et al.*, 2001; *Chin et al.*, 2002; *Chuang et al.*, 2002; *Liao et al.*, 2003] facilitates a more detailed investigation of the photochemical effects of aerosols on tropospheric O_3 and OH. We present here such an investigation using a global 3-D model of tropospheric chemistry (GEOS-CHEM). Section 2 describes the implementation of aerosol photochemistry in GEOS-CHEM and section 3 examines its implications. Section 4 compares the results with observations for species and regions where the effects are particularly large. Global budgets of O_3 and OH are analyzed in section 5.

2. GEOS-CHEM Model

2.1. General Formulation

[5] The GEOS-CHEM model was initially described by *Bey et al.* [2001a] and subsequent improvements are described by *Martin et al.* [2002b]. We use here GEOS-CHEM version 4.26 (http://www-as.harvard.edu/chemistry/trop/geos/) with improved treatment of aerosol photochemical effects and a few other updates as described below. The model is driven by assimilated meteorological data from the Goddard Earth Observing System (GEOS) of the NASA Data Assimilation Office (DAO) [*Schubert et al.*, 1993]. The meteorological data include 3-D fields updated every 3 hours for surface fluxes and mixing depths and every 6 hours for other relevant variables. We use for this study the GEOS data for 1996–1997, available with a resolution of 2° latitude by 2.5° longitude and 46 sigma levels in the vertical extending up to 0.1 hPa. For computational expedience we degrade the horizontal resolution to 4° latitude by 5° longitude and merge the vertical levels above the lower stratosphere, retaining a total of 26. There are five levels located below 2 km altitude (for a column based at sea level, these levels are centered at 50 m, 250 m, 600 m, 1100 m, and 1700 m).

[6] The GEOS-CHEM model includes a detailed description of tropospheric O_3-NO_x-hydrocarbon chemistry. It solves the chemical evolution of about 120 species with a Gear solver [*Jacobson and Turco*, 1994] and transports 24 tracers. Photolysis frequencies are computed using the Fast-J radiative transfer algorithm [*Wild et al.*, 2000] which includes Rayleigh scattering as well as Mie scattering by clouds and aerosols. Extensive evaluations of the GEOS-CHEM chemical fields with observations of tropospheric O_3 and its precursors in different regions of the world have been presented in a number of papers [e.g., *Bey et al.*, 2001a, 2001b; *Li et al.*, 2001, 2002a, 2002b; *Palmer et al.*, 2001, 2003; *Chandra et al.*, 2002; *Fiore et al.*, 2002; *Liu et al.*, 2003; *Martin et al.*, 2002a, 2002b]. Observed monthly mean O_3 concentrations in different regions of the troposphere are usually reproduced to within 10 ppbv with no global bias, but there are some regional problems, most prominently a 20–30 ppbv positive bias over India [*Martin et al.*, 2002b]. The seasonal and interannual variability of CO is well captured, but there is a general negative bias of 10–20 ppbv in the Northern Hemisphere. Consideration of aerosol photochemical effects alleviates these discrepancies, as discussed in section 4.

[7] The model version used here includes several updates to the version presented by *Martin et al.* [2002b], in addition to the aerosol effects described below. The most important are updated reaction rates for organic peroxy radicals [*Tyndall et al.*, 2001], updated CO emissions (B.N. Duncan et al., Model study of the variability and trends of carbon monoxide (1988–1997), 1, Model formulation, evaluation, and sensitivity, manuscript in preparation, 2002), and updated acetone emissions [*Jacob et al.*, 2002]. Also, surface emissions of trace gases are now distributed vertically in the unstable mixed layer (which can vary from less than 100 m at night to over 2000 m during the day) to minimize numerical artifacts from operator splitting (1-hour time steps between chemistry and transport).

2.2. Aerosol Radiative and Chemical Effects

[8] Previous versions of GEOS-CHEM have included heterogeneous reactions of HO_2, NO_2, NO_3, and N_2O_5 in sulfate aerosols [*Bey et al.*, 2001a], and more recently these same reactions as well as radiative effects have been included for mineral dust aerosols [*Martin et al.*, 2002b]. We include here a more comprehensive treatment of the photochemical effects of aerosols. To this end we use global 3-D monthly mean fields for 1996–1997 of dry aerosol mass from the GOCART model [*Chin et al.*, 2000a, 2000b, 2002; *Ginoux et al.*, 2001] which uses the same GEOS meteorological fields and transport algorithms as GEOS-CHEM. The GOCART data include sulfate, size-resolved mineral dust and sea salt, hydrophobic and hydrophilic black carbon, as well as hydrophobic and hydrophilic organic carbon. Nitrate aerosol is not included.

[9] As described in detail elsewhere [*Chin et al.*, 2000a, 2002; *Ginoux et al.*, 2001], the GOCART model sulfate simulation includes oxidation of SO_2 emitted from industrial activity, biomass burning, biofuel, volcanic eruptions, and formed from dimethylsulfide (DMS) released from the ocean, as well as a small direct sulfate source. Oxidation rates in the GOCART model are calculated with offline fields of OH and aqueous H_2O_2. Organic and black carbon are emitted directly from biomass burning and industrial activity, with 80% of black carbon and 50% of organic carbon emitted as hydrophobic, the rest being hydrophilic. Organic carbon is also formed from volatile organic compounds. Hydrophobic carbonaceous aerosols age to become hydrophilic with an e-folding time of 1.2 days. Mineral dust emission is calculated as a function of the local probability of bare sediments, surface wind speed, and surface wetness. Sea-salt emission is calculated as a function of surface wind speed. All aerosols are subject to dry deposition and hydrophilic aerosols to wet deposition.

[10] Simulation of the radiative and chemical effects of aerosols requires information on the relative humidity (RH) dependent aerosol size distribution. We obtain this information from *Ginoux et al.* [2001] for mineral dust, and from the Global Aerosol Data Set (GADS) [*Köpke et al.*, 1997] and *Chin et al.* [2002] for other aerosols, and apply it to local RH from the GEOS fields. Table 1 shows the hygroscopic growth factors and Table 2 shows the effective radius r_e at 70% humidity. The effective radius is defined as $\int_r \pi r^3 f(r) dr / \int_r \pi r^2 f(r) dr$, where $f(r)$ is the fraction of par-

Table 1. Hygroscopic Growth Factors for Aerosols[a]

	RH, %				
	0	50	70	80	90
Sulfate	1.0	1.4	1.5	1.6	1.9
Black carbon[b]	1.0	1.0	1.0	1.2	1.4
Organic carbon[b]	1.0	1.2	1.4	1.5	1.7
Sea salt	1.0	1.6	1.8	2.0	2.4
Mineral dust[c]	1.0	1.0	1.0	1.0	1.0

[a]The hygroscopic growth factor is the ratio of the wet to the dry effective radius.

[b]These are values for hydrophilic aerosols. There is no hygroscopic growth for hydrophobic carbon aerosols.

[c]Dust particles are sufficiently large, and their hygroscopicity sufficiently low, that hygroscopic growth is considered negligible [*Li-Jones et al.*, 1998].

ticles with radius between r and $r + dr$ [*Hansen and Travis*, 1974]. We cap aerosol growth above 90% RH; hygroscopic growth is very nonlinear at higher RH and cannot be adequately resolved in the GEOS fields because of subgrid-scale variability, especially associated with clouds.

[11] Calculation of the radiative effects of aerosols also requires information on the wavelength-dependent complex refractive index. We obtain this information from *Patterson et al.* [1977] for mineral dust, and for other aerosols as a function of RH from GADS. We assume an external mixture of the different aerosol types. *Pósfai et al.* [1999] found that soot and sulfate aerosols are often internally mixed; *Liao et al.* [1999] calculated that the absorbing effect of aerosols on photolysis frequencies is 5–15% larger for internally versus externally mixed sulfate-soot aerosols. A more physically realistic treatment of mixed sulfate-soot aerosols as a black carbon core surrounded by sulfate would have an intermediate effect [*Jacobson*, 2000].

[12] We use a Mie algorithm [*de Rooij and van der Stap*, 1984; *Mishchenko et al.*, 1999] to calculate for each aerosol type the single scattering albedo, the extinction efficiency, and the first eight terms in the Legendre expansion of the phase function, for input to the Fast-J radiative transfer code of *Wild et al.* [2000]. We tabulate the optical properties at the RH values in Table 1, and interpolate in the simulation. Table 2 shows the resulting optical properties at 0.4 μm and 70% RH. Sulfate and sea salt are purely scattering, black carbon is strongly absorbing, and organic carbon is moderately absorbing at UV and visible wavelengths. Organic carbon aerosols could be highly absorbing in the UV if they contain chromophore functional groups [*Jacobson*, 1999], but this is not considered here. Mineral dust is strongly absorbing in the UV and moderately absorbing at visible wavelengths. The extinction efficiencies of black carbon, organic carbon, and sulfate are about 20–60% larger at 300 nm than at 400 nm. The extinction efficiencies of supermicron mineral dust and sea-salt particles exhibit little wavelength sensitivity at UV and visible wavelengths.

[13] We calculate the aerosol optical depth locally in the model from the mass concentration, extinction efficiency, and particle mass density for each particle type and wavelength. Figure 1 shows the modeled aerosol optical depth at 400 nm during March and August. Extensive evaluation of the GOCART fields with in situ, ground based, and satellite observations have been presented in a number of papers [*Chin et al.*, 2000b, 2002; *Ginoux et al.*, 2001; *Penner et al.*, 2001; S. Kinne et al., Monthly averages of aerosol properties: A global comparison among models, satellite data and AERONET ground data, submitted to *Journal of Geophysical Research*, 2002]. The GOCART aerosol fields are generally consistent with observations to within a factor of 2. Mineral dust and sulfate dominate the background optical depth in the Northern Hemisphere. Mineral dust optical depth reaches a seasonal maximum during boreal summer, associated with surface cyclones that erode particles from topographic depressions in desert regions and with intense solar heating that transports particles into the free troposphere through dry convection [*Ginoux et al.*, 2001]. The mineral dust optical depth of greater than 0.5 over much of northern Africa during summer is consistent with measurements from AERONET [*Holben et al.*, 2001] and retrievals from TOMS [*Torres et al.*, 2002], as shown by *Ginoux et al.* [2001] and *Chin et al.* [2002]. Mineral dust over the tropical Pacific is biased high by a factor of 2–5 [*Ginoux et al.*, 2001]. Sulfate optical depth is maximum during summer due to higher SO_2 oxidation rates, and is most important over the eastern United States, eastern Asia, and Europe [*Chin et al.*, 2000a, 2000b]. Modeled sulfate concentrations over the eastern United States are a factor of 1.5 lower than observations from the Eulerian Model Evaluation Field Study (EMEFS) [*Chin et al.*, 2000b]. Black and organic carbon aerosols from biomass burning contribute to seasonal enhancements in optical depth over South Asia during March and southern Africa during August [*Kuhlbusch et al.*, 1996; *Chowdhury et al.*, 2001; *Holben et al.*, 2001; *Leon et al.*, 2001]. The GOCART model optical depths are generally within 0.3 of AERONET measurements over African biomass burning regions, but are about 2–3 times lower than AERONET measurements over the biomass burning region of South America [*Chin et al.*, 2002]. Black carbon is also notable over northern Europe (diesel engines) and East Asia (biofuels). Sea-salt

Table 2. Aerosol Optical Properties at 0.4 μm Wavelength (RH = 70%)[a]

Aerosol Type	Density, g cm^{-3}	r_e, μm	Refractive Index	ϖ_o	Q
Sulfate	1.7	0.24	$1.36-10^{-8}i$	1.00	1.95
Black carbon	1.0	0.04	$1.75-0.46i$	0.27	0.76
Organic carbon	1.8	0.10	$1.42-0.002i$	0.98	0.74
Sea salt[b]					
Accumulation	2.2	1.3	$1.37-10^{-8}i$	1.00	2.43
Coarse	2.2	10.1	$1.37-10^{-8}i$	1.00	2.09
Mineral dust[b]					
0.1–0.18 μm	2.5	0.15	1.58–0.014i	0.94	2.48
0.18–0.3 μm	2.5	0.25	1.58–0.014i	0.91	3.10
0.3–0.6 μm	2.5	0.4	1.58–0.014i	0.86	2.82
0.6–1 μm	2.5	0.8	1.58–0.014i	0.76	2.43
1–1.8 μm	2.65	1.5	1.58–0.014i	0.68	2.27
1.8–3 μm	2.65	2.5	1.58–0.014i	0.62	2.19
3–6 μm	2.65	4.0	1.58–0.014i	0.58	2.14

[a]Effective radius r_e, single scattering albedo ϖ_o, and extinction efficiency Q are calculated using refractive index and lognormal size distribution data available from the Global Aerosol Data Set (GADS) [*Köpke et al.*, 1997] and *Chin et al.* [2002] with the following exceptions. We use a geometric standard deviation of 2.0 for all aerosol types except mineral dust. The calculations for mineral dust use complex refractive indices from *Patterson et al.* [1977], and assume a standard gamma particle size distribution with effective variance of 0.2.

[b]Size ranges were resolved in the GOCART simulation and used as input to GEOS-CHEM.

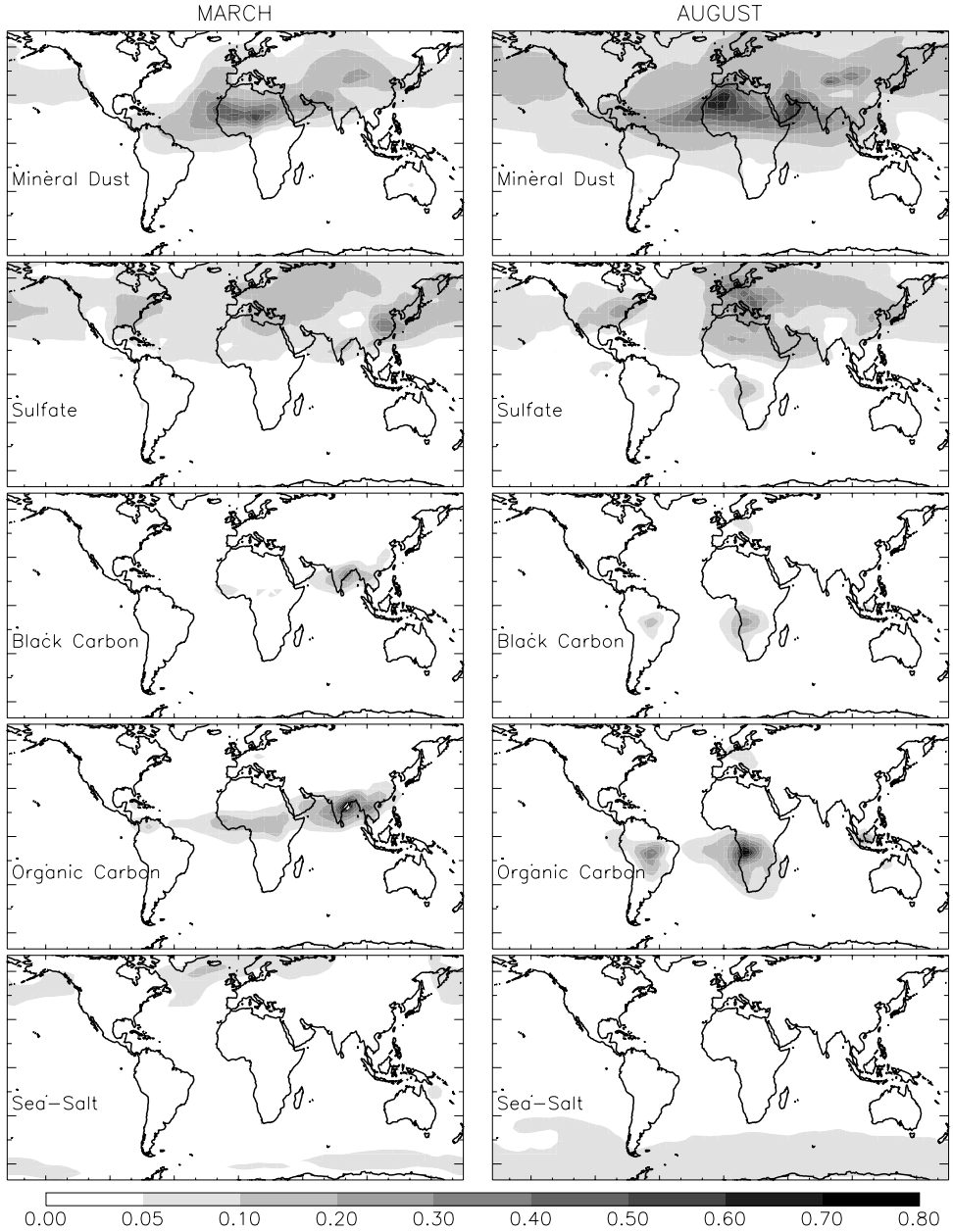

Figure 1. Modeled monthly mean optical depth at 400 nm of different aerosol types for March 1997 (left column) and August 1997 (right column). Values are calculated from mass concentration fields from *Ginoux et al.* [2001] for mineral dust and from *Chin et al.* [2002] for the other aerosol types. See color version of this figure at back of this issue.

optical depths are highest near ±60° where strong surface winds increase emissions [*Gong et al.*, 1997].

[14] We implement heterogeneous chemistry on aerosol surfaces in GEOS-CHEM following a standard reaction probability formulation. We neglect heterogeneous chemistry in clouds which would be difficult to constrain in our coarse resolution model; its effect on O_3 and OH is limited in any case by the small fraction of atmospheric volume occupied by clouds [*Liang and Jacob*, 1997]. As pointed out by *Jacob* [2000] it is the atmospheric volume fraction occupied by clouds, rather than the frequency of cloud processing, that limits the effect of cloud chemistry on the global budgets of O_3 and OH.

[15] In the reaction probability formulation, the rate constant k for chemical loss of a gas with mean molecular speed v and gas-phase molecular diffusion coefficient D_g on an aerosol of particle radius a is given by

$$k = \left(\frac{a}{D_g} + \frac{4}{v\gamma}\right)^{-1} A \qquad (1)$$

where γ is the reaction probability, i.e., the probability that a molecule impacting the aerosol surface undergoes reaction [*Ravishankara*, 1997], and A is the aerosol surface area per unit volume of air. We calculate D_g as a function of

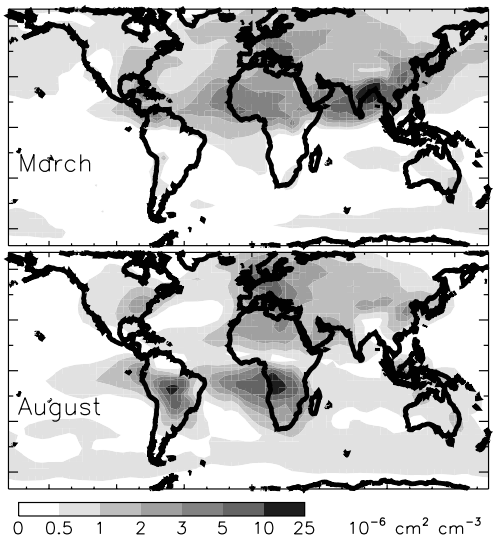

Figure 2. Modeled monthly mean total aerosol surface area in the lower troposphere (~600 m above the surface) for March and August 1997. Values are calculated from mass concentration fields from *Ginoux et al.* [2001] for mineral dust and from *Chin et al.* [2002] for the other aerosol types. See color version of this figure at back of this issue.

molecular weight, temperature, and air density following *Dentener* [1993]. We include the four heterogeneous reactions $HO_2 \rightarrow 0.5\ H_2O_2$, $NO_2 \rightarrow 0.5\ HONO + 0.5\ HNO_3$, $NO_3 \rightarrow HNO_3$, and $N_2O_5 \rightarrow 2\ HNO_3$ with reaction probabilities of 0.2, 10^{-4}, 10^{-3}, and 0.1, respectively, as recommended by *Jacob* [2000]. The products have long lifetimes relative to the timescales for gas-particle exchange and are therefore released into the gas phase. Uptake of NO_2 on dry dust surfaces may be less (10^{-6}–10^{-4}) [*Grassian*, 2001], but the phase of mineral dust surfaces in the atmosphere is unclear [*Martin*, 2000]. For the range of r_e and γ values used here, the chemical rate constant k may be limited either by free molecular collision ($4/v\gamma$ term in equation (1)) or by diffusion (a/D_g term). Figure 2 shows the aerosol surface area in the lower troposphere (~600 m). The spatial distribution is similar to that of optical depth but features stronger maxima in regions where submicron aerosols dominate.

[16] We do not include reactive uptake of O_3 by aerosols, for which *Jacob* [2000] cites no conclusive laboratory or field evidence. *Dentener et al.* [1996] postulated direct uptake of O_3 by dust with an assumed γ_{03} of 10^{-4}–10^{-5} based on analogy with measured O_3 deposition to bare soil. However, O_3 deposition to soil most likely involves reaction with unsaturated organics. Laboratory measurements show that O_3 uptake by organic aerosol surfaces is rapidly quenched as surface reaction sites are oxidized [*Moise and Rudich*, 2000]. Recent laboratory measurements on dry mineral dust surfaces reveal $\gamma_{03} \sim 10^{-5}$ with no apparent surface saturation, but with a factor of 2–3 decrease over several hours of exposure [*Michel et al.*, 2002]. A model study of an African dust layer over the Atlantic by *De Reus et al.* [2000] indicates that reactive uptake of O_3 ($\gamma = 5 \times 10^{-5}$) would reduce simulated O_3 concentrations in the layer by 11 ppbv, improving agreement with observations. Further work is evidently needed on this issue.

[17] We also do not include reactive uptake of CH_3O_2, HCHO, HNO_3, or H_2O_2 by aerosols. Current evidence is that uptake of CH_3O_2 and HCHO is too slow to be of atmospheric significance [*Jacob*, 2000]. Uptake of HNO_3 by alkaline dust particles is important for the partitioning of HNO_3 between the aerosol and gas phase, but should have little impact on oxidant concentrations since both HNO_3(g) and nitrate aerosols are removed by wet deposition. *De Reus et al.* [2000] calculated that uptake of HNO_3 had a large role only if the HNO_3 in the aerosol phase was not permitted to regenerate NO_x through photolysis. Uptake of H_2O_2, if determined by reaction with SO_2, is significant only in clouds and has little overall effect on HO_x [*Tie et al.*, 2001].

[18] We use a March 1996 to August 1997 simulation period. The first 6 months are used to achieve proper initialization and we present results for September 1996 to August 1997. Biomass burning emissions for that period are specified from satellite observations [*Duncan et al.*, 2003] (the large fires in Oceania associated with El Niño have not yet begun). The standard simulation is as described above. A sensitivity simulation is conducted that excludes both the radiative effects of aerosols and the heterogeneous uptake of HO_2, NO_2, and NO_3 (but retains the uptake of N_2O_5). Additional simulations focused on the effects of mineral dust for the same time period were presented by *Martin et al.* [2002b]. We also perform 1-month sensitivity simulations (following a 1-month spin-up) for March and August 1997 to compare the relative importance of radiative and chemical effects of aerosols.

3. Photochemical Effects of Aerosols

[19] Figure 3 shows that aerosols reduce UV photolysis frequencies near the surface throughout a large part of the world. The noontime $O_3 \rightarrow O(^1D)$ photolysis frequency, $J(O(^1D))$ (300–320 nm), decreases by more than 5% over most of the Northern Hemisphere, largely due to mineral

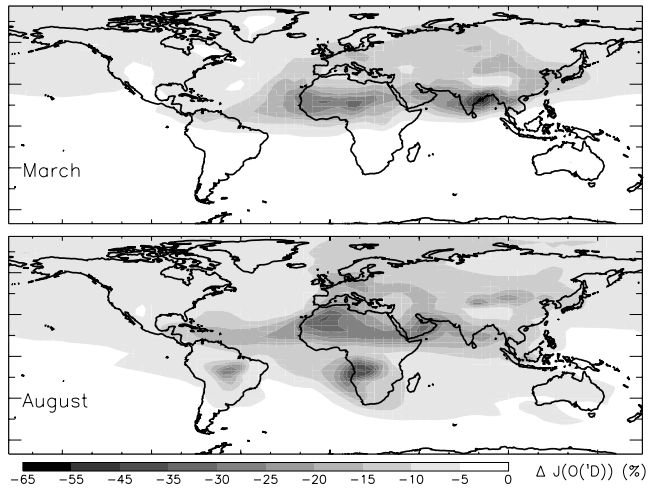

Figure 3. Sensitivity to aerosols of the $O_3 \rightarrow O(^1D)$ photolysis frequency ($J(O(^1D))$) in surface air. Values are monthly mean model results for March and August 1997. See color version of this figure at back of this issue.

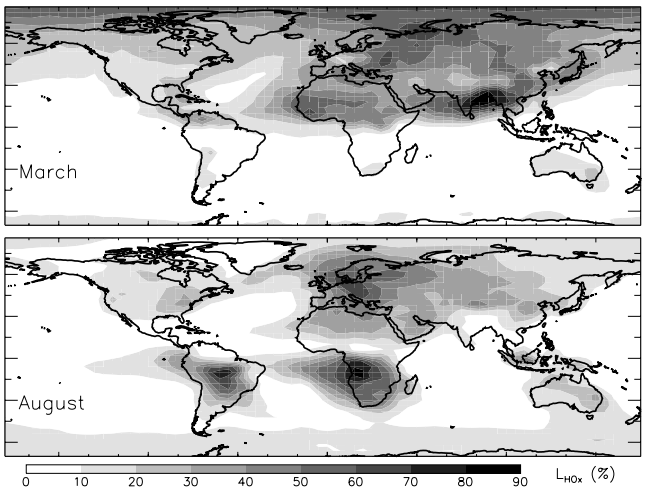

Figure 4. Fraction of total HO_x loss in the lower troposphere (~600 m above the surface) contributed by uptake of HO_2 by aerosols. Values are monthly mean model results for March and August 1997. See color version of this figure at back of this issue.

dust. The effect on $J(NO_2)$ (340–400 nm) is similar to that on $J(O(^1D))$ and about 10% weaker. Removing sulfate from the aerosol mixture generally causes a slight increase (<2%) in $J(O(^1D))$ relative to the standard simulation near the surface; 1-D calculations by *Liao et al.* [1999] similarly showed that in the presence of absorbing aerosols, sulfate aerosols have a small effect on photolysis frequencies. Mineral dust reduces $J(O(^1D))$ by 15–30% over and downwind of northern Africa throughout the year [*Martin et al.*, 2002b]. Black carbon causes most of the 15–25% decrease in $J(O(^1D))$ over northern Europe during August. Aerosols from biomass burning and other sources in the Ganges Valley reduce $J(O(^1D))$ near the surface by a factor of 2, largely due to black carbon with smaller contributions from organic carbon and mineral dust. Similar features are observed over southern Africa during August. The reduction in photolysis frequencies may be 5–15% greater for internally mixed aerosols than for the external mixture assumed here [*Liao et al.*, 1999]. Measurements of $J(O(^1D))$ over the northern Indian Ocean during March showed reductions of 40% due to absorbing aerosols (J. Burkert et al., Trace gas and radical diurnal behavior in the marine boundary layer during INDOEX 1999, submitted to *Journal of Geophysical Research*, 2002), consistent with the results presented here.

[20] Heterogeneous chemistry also contributes to the photochemical effects of aerosols. Figure 4 shows the fraction of total HO_x loss in the lower troposphere (~600 m altitude) contributed by aerosol uptake of HO_2. Here we define total HO_x loss as the sum of the main loss pathways [*Frost et al.*, 1998; *Jaeglé et al.*, 2001]: $2(OH + HO_2) + 2(HO_2 + HO_2) + 2(HO_2 + CH_3O_2) + (NO_2 + OH) + 2(HNO_4 + OH)$ + aerosol uptake of HO_2. Aerosols are responsible for more than 70% of HO_x loss over biomass burning regions. The abundance of fine aerosol over biomass burning regions [*Anderson et al.*, 1996] and industrial regions [*ten Brink et al.*, 1997] leads to high aerosol surface area and rapid gas-particle mass transfer (this transfer is not diffusion-limited, unlike with supermicron particles). Aerosol uptake of HO_2 is responsible for over 50% of HO_x loss over Eastern Europe during August, due to high surface areas from organic carbon (anthropogenic and biogenic) and sulfate, both of which peak in the summer. Black carbon constitutes less than 20% of total surface area over Eastern Europe, despite playing a dominant role in the reduction of photolysis rates. Uptake of HO_2 by aerosols accounts for over 20% of HO_x loss over much of northern Africa, the Atlantic Ocean, and Asia, and over 50% of HO_x loss in the Arctic during March.

[21] Figure 5 shows the fraction of total NO_x loss to HNO_3 contributed by aerosol uptake of NO_2 and NO_3 in the lower troposphere for March and August. This fraction is 15–30% in regions with high concentrations of biomass burning, mineral dust, and sea-salt aerosols. Over land, heterogeneous NO_x loss is mainly NO_2 uptake. Over oceans, uptake of NO_2 and NO_3 have comparable roles. We do not include reaction of NO_3 with marine DMS in the model, and as a result may exaggerate the importance of NO_3 heterogeneous uptake over the oceans.

[22] We examine the vertical distribution of the photochemical effects of aerosols over two regions where the effects are large: during March over India where carbonaceous aerosols are particularly important and during August over the Sahara where mineral dust dominates. The vertical profile of the radiative effect is shown in the top panels of Figure 6. The effect decreases rapidly with altitude following the distribution of aerosols. The small enhancement in $J(NO_2)$ in the upper troposphere over India results from scattering by aerosols below. The middle panels of Figure 6 show the vertical profiles of the chemical effect of aerosols. Uptake of HO_2 on aerosol surfaces is responsible for about 80% of HO_x loss through the depth of the boundary layer over India, and 20–40% of HO_x loss throughout most of the troposphere over the Sahara. Almost 20% of the HNO_3 production in the boundary layer over India results from uptake of NO_2 by aerosols. The bottom panels in Figure 6 show that over India the radiative and chemical properties

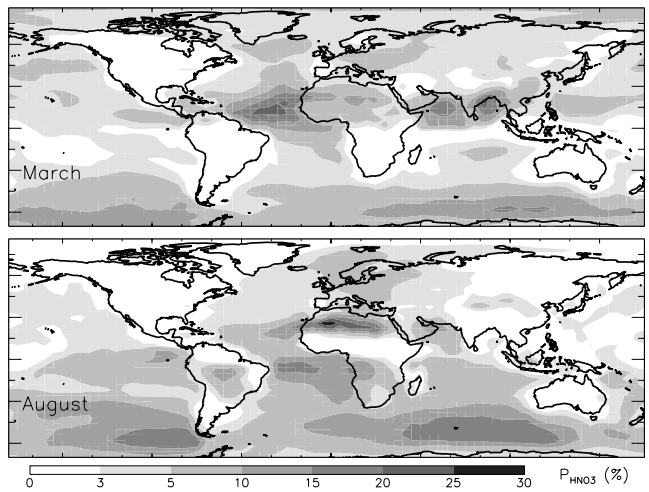

Figure 5. Fraction of total HNO_3 production in the lower troposphere (~600 m above the surface) contributed by uptake of NO_2 and NO_3 by aerosols. Values are monthly mean model results for March and August 1997. See color version of this figure at back of this issue.

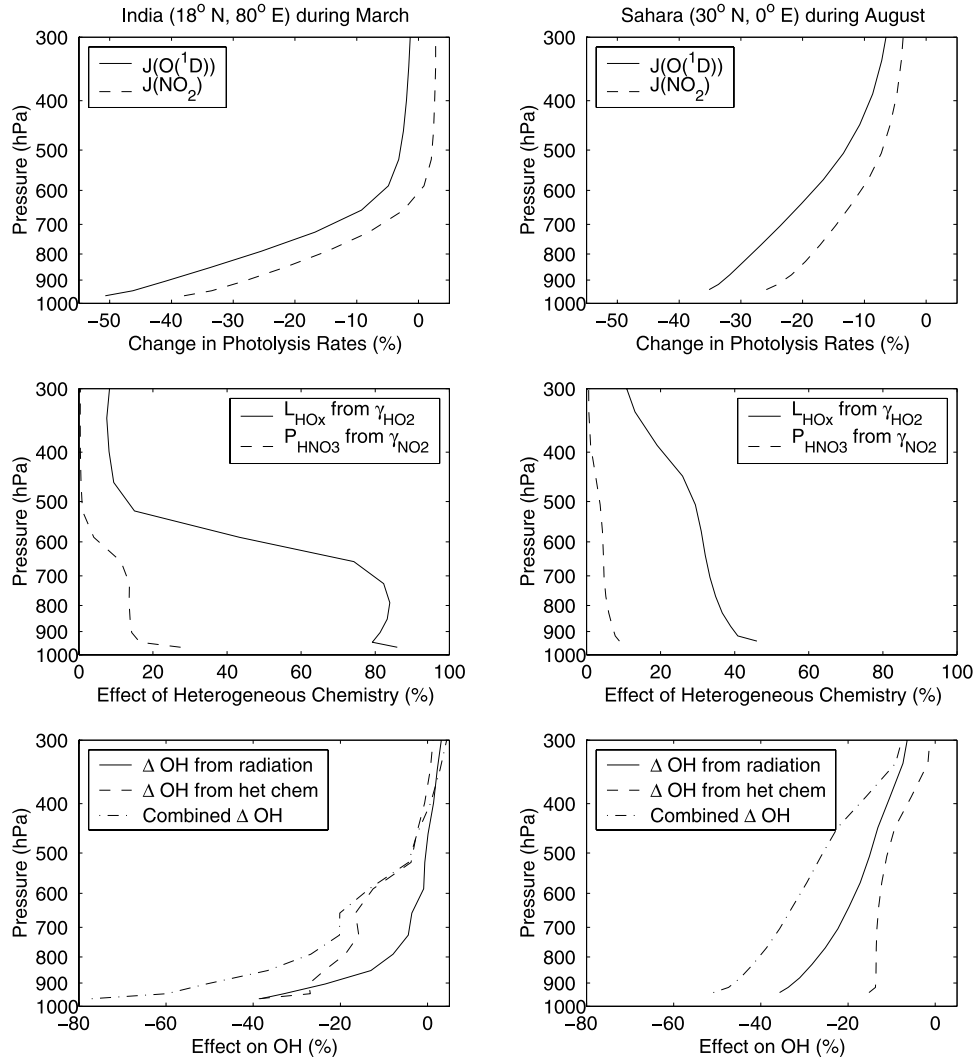

Figure 6. Photochemical effects of aerosols over India and the Sahara. Values are monthly mean model results. (top) Effects on $J(O(^1D))$ and $J(NO_2)$. (middle) Fraction of total HO_x loss contributed by aerosol uptake of HO_2 and the fraction of total HNO_3 production contributed by aerosol uptake of NO_2 and NO_3. (bottom) Effect of these radiative and heterogeneous processes on OH concentration as determined by difference with simulations that did not include either or both of these processes.

of aerosols have comparable effects on OH near the surface, but chemical effects dominate at higher altitudes where the overhead aerosol column is smaller. Over the Sahara the radiative effects of mineral dust are about twice as important as the chemical effects, reflecting the absorbing nature of mineral dust at UV wavelengths [*Sokolik et al.*, 1993] and the large size of the dust particles.

[23] Figure 7 shows the combined photochemical effects of aerosols on OH, CO, NO_x, and O_3 concentrations in March. Here we compare the standard simulation to a simulation excluding radiative effects of aerosols and the heterogeneous reactions of HO_2, NO_2, and NO_3 (hydrolysis of N_2O_5 is included in both simulations). The top panel shows that OH is reduced by 25–50% over northern Africa and South Asia, largely due to mineral dust, organic carbon, and black carbon. Over northern India near Calcutta, OH decreases by a factor of 4 reflecting comparable contributions from radiative and chemical effects. Over much of the Northern Hemisphere OH concentrations decrease by 5–25%; about half of this decrease is from the radiative effects of mineral dust. The depletion of OH increases the lifetime of CO and other trace gases such as NO_x and non-methane hydrocarbons, increasing their export from regions of emissions. As a result, CO increases by 5–15 ppbv (5–10%) throughout much of the Northern Hemisphere, with local increases downwind of biomass burning regions of 20–75 ppbv (10–15%). Ship and aircraft measurements during the March winter monsoon found elevated CO concentrations in the marine boundary layer off the coast of India [*Rhoads et al.*, 1997; *Lelieveld et al.*, 2001]; our analysis suggests that depletion of OH by aerosols contributed to the observed enhancement. Over the tropical Atlantic downwind of the Sahara, CO increases by 10–20 ppbv (7–13%).

[24] The photochemical effects of aerosols generally result in a slight increase of NO_x over continental regions due to OH depletion. Over the oceans the effect is more often a slight decrease (up to 20%) as NO_2 and NO_3 uptake are relatively more important (Figure 5). The bottom panel

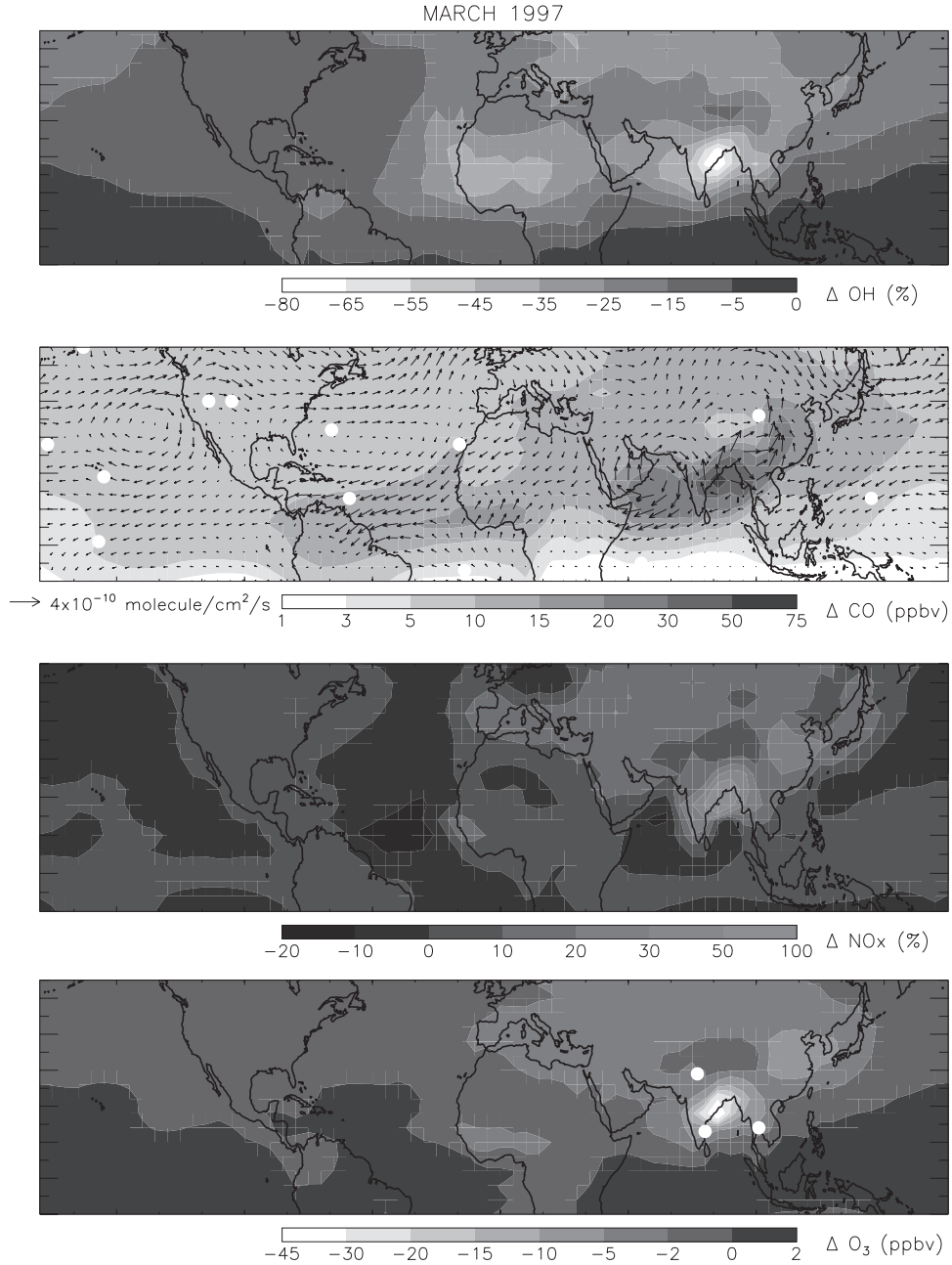

Figure 7. Changes in OH, CO, NO_x, and O_3 concentrations in the lower troposphere (~600 m above the surface) from scattering and absorption by aerosols, and from uptake of HO_2, NO_2, and NO_3 by aerosols, as determined by difference with a simulation that did not include these effects. Values are model monthly means during March. White circles show the locations of observations compared to the model in section 4. Also shown is the change in the CO flux due to the above aerosol effects. See color version of this figure at back of this issue.

shows that the effect on O_3 is confined largely to regions with intense emissions of both aerosols and O_3 precursors. Ozone is reduced by 10–40% or 15–45 ppbv over and downwind of the biomass burning region of northern India during March. Ozone also is reduced by 5–10 ppbv (10–15%) over northeastern China and the Yellow Sea, a region where industrial activity is collocated with high aerosol loading from anthropogenic and mineral dust aerosols [*Zhang et al.*, 1994; *Zhang and Carmichael*, 1999]. *Phadnis and Carmichael* [2000] previously used a regional 3-D model to calculate a reduction in boundary layer O_3 of about 5% over the region during May due to uptake of HO_2 ($\gamma = 0.1$), H_2O_2 ($\gamma = 0.1$), N_2O_5 ($\gamma = 0.1$), and HNO_3 ($\gamma = 0.1$) on mineral dust.

[25] Figure 8 shows the same results but for August. The top panel shows that OH is reduced by 25–40% over Europe, largely from the radiative and chemical effects of sulfate, black carbon, and organic carbon. Similar reductions in OH over northern Africa and parts of Asia occur primarily from the radiative effects of mineral dust. About

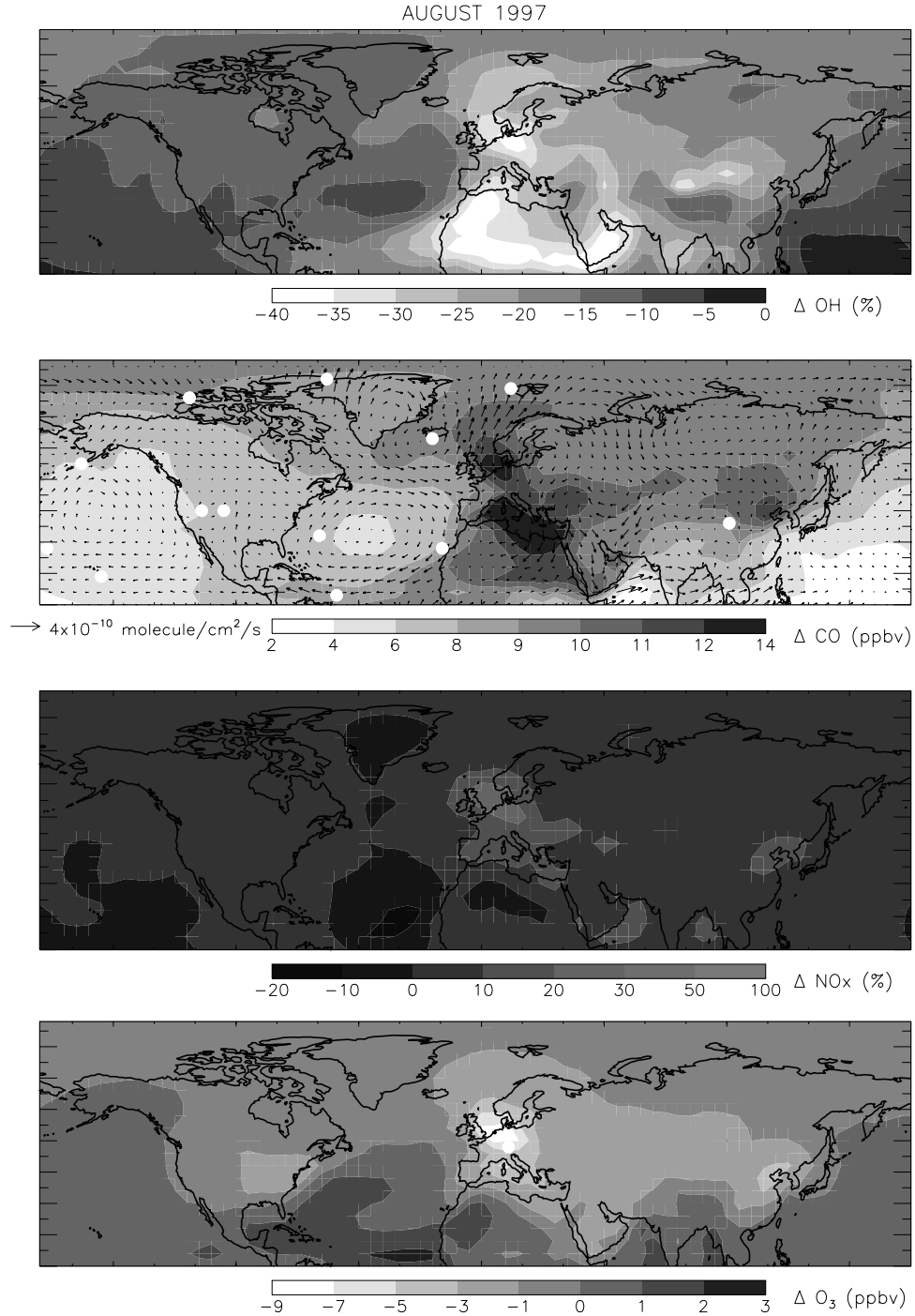

Figure 8. As in Figure 7, but for August. See color version of this figure at back of this issue.

half of the reduction of 5–25% over most of the Northern Hemisphere is from the radiative effects of mineral dust. Concentrations of CO increase by 5–10 ppbv throughout much of the Northern Hemisphere, with local increases of more than 10 ppbv over Europe and the Mediterranean. Concentrations of NO_x generally increase by less than 10%, with local increases of up to 30% over Europe, and local decreases of up to 20% over tropical oceans. As for March the effect on O_3 is localized to photochemically active regions where aerosols are collocated with anthropogenic emissions of O_3 precursors. Aerosols reduce O_3 in the boundary layer by 5–9 ppbv over northern Europe during August 1997. We find a smaller reduction in July 1997 (3–5 ppbv) due to lower aerosol loadings, which in the model are due to higher precipitation. The photochemical effects of aerosols are smaller over the eastern United States where concentrations of absorbing aerosols are lower. The combined photochemical effects of aerosols decrease O_3 in the boundary layer over the eastern United States by up to 3 ppbv and over East Asia by up to 5 ppbv.

[26] Comparison of our results with previous global model studies of sensitivity to aerosol photochemistry is

Table 3. Aerosol Processes Examined in Previous Global Sensitivity Studies

Aerosol Types Included (X)					Reactions Examined[a]								
SO_4^{2-}	BC[b]	OC[c]	SS[d]	Dust	γ_{N2O5}	γ_{HO2}	γ_{NO2}	γ_{NO3}	γ_{O3}	γ_{HNO3}	γ_{HCHO}	$h\nu$[e]	Reference
X			X		0.1			0.1					[*Dentener and Crutzen*, 1993]
				X	0.1	0.1			$1-20 \times 10^{-5}$	0.1			[*Dentener et al.*, 1996]
X	X				0.1	0.2–0.5			$7-300 \times 10^{-5}$		0.01–0.02		[*Tie et al.*, 2001]
X	X	X		X	0.1	0.2	10^{-4}	10^{-3}	5×10^{-5}	0.1		X	[*Liao et al.*, 2003]
				X	0.1	0.2	10^{-4}	10^{-3}				X	[*Martin et al.*, 2002a, 2002b]
X	X	X	X	X		0.2	10^{-4}	10^{-3}				X	This work

[a]Uptake rates shown only for reactions examined in separate sensitivity simulations.
[b]Black carbon.
[c]Organic carbon.
[d]Sea salt.
[e]Scattering and absorption of ultraviolet radiation by aerosols.

difficult because of differences in the aerosol processes and aerosol types examined. Table 3 shows these differences. *Liao et al.* [2003] find that the radiative effects of aerosols change O_3 concentrations by less than 1 ppbv anywhere in a global 3-D model with substantially smaller aerosol loadings than used here. *Dickerson et al.* [1997] calculated that the radiative effects of aerosols increase surface O_3 over regions of scattering aerosols such as the eastern United States, and decrease O_3 over regions of absorbing aerosols. We find that the combined radiative and chemical effects of aerosols lead to small net decreases in O_3 over the eastern United States, and larger decreases in O_3 over Europe and Asia where aerosols are more absorbing. *Tie et al.* [2001] calculated that uptake of HO_2 ($\gamma = 0.2$) by sulfate aerosols decreases zonal mean OH by 5–10% during June north of 45°N. Over this region sulfate aerosols are the largest contributor to the aerosol load; our results are comparable to those of *Tie et al.* [2001] and indicate that consideration of radiative effects would about double the impact on OH. *Dentener et al.* [1996] found that uptake of HO_2 ($\gamma = 0.1$) by mineral dust decreased HO_2 concentrations over northern Africa and the Gobi Desert by up to 10% during February, March, and April, but had little effect on O_3 due to low NO_x concentrations. Over this region where mineral dust dominates the total aerosol load, we calculate an effect on HO_2 four times as large using γ_{HO2} of 0.2 and accounting for scattering and absorption of UV radiation by mineral dust. The effect on O_3 is still small.

4. Comparison With Observations

[27] We compared our model results with a suite of aircraft, sonde, and satellite observations to determine if inclusion of the photochemical effects of aerosols described here improves or degrades the simulation. Again these effects include (1) absorption and scattering of ultraviolet radiation and (2) reactive uptake of HO_2, NO_2, and NO_3. We present here selected comparisons for locations where the model exhibits large discrepancies with observations and where aerosol effects are large. Large decreases in O_3 are found over South Asia in March and northern Europe in August due to photochemical effects of aerosols (Figures 7 and 8). Figure 9 compares monthly mean modeled O_3 profiles over South Asia with measurements from commercial aircraft as part of the Measurement of Ozone and Water Vapor by Airbus In-Service Aircraft (MOZAIC) program [*Marenco et al.*, 1998] during 1995–1999. The photochemical effects of aerosols improve the simulation at all three sites by decreasing O_3 concentrations in the lower troposphere, although they have minimal effect at higher altitudes (above 600 hPa) where the model is still too high. The magnitude of the lower tropospheric correction, although insufficient to bring model results in agreement with observations, is correlated with the magnitude of the model bias. The low O_3 values observed at Madras in surface air likely reflect local titration. *Lal and Lawrence* [2001] found a model overestimate of comparable magnitude at the surface during February and March at Ahmedabad (23°N, 73°E). Our black carbon emissions from fossil fuels in India [from *Cooke et al.*, 1999] may be a factor of 2–3 too low [*Dickerson et al.*, 2002], so that aerosols may reduce O_3 over India throughout the year and may lead to a greater O_3 reduction during March. However, it does not appear that aerosols could correct the model overestimate above 600 hPa.

[28] Figure 10 compares simulated and observed (sondes) ozone profiles at Hohenpeissenberg in northern Europe (43°N, 11°E, 975 m altitude) in August. Topography complicates the comparison between GEOS-CHEM and ozonesondes near the surface, but the comparison at 800 hPa shows that aerosols reduce the model bias. There is a negative model bias for that site in the free troposphere for which aerosols offer no explanation. We calculate that aerosols decrease surface O_3 over the eastern United States by 1–3 ppbv, which could correct our previously reported model bias of 3–5 ppbv in the region [*Fiore et al.*, 2002].

[29] Figure 11 shows that consideration of the photochemical effects of aerosols increases CO by 2–5 ppbv at most tropical sites, by 5–10 ppbv at remote sites in the northern midlatitudes, and by about 10 ppbv in the Arctic, improving agreement with observations and removing the model bias in the extratropics. We find relatively little influence on the seasonal variation of CO.

5. Global Budgets of O_3 and OH

[30] Table 4 shows annual mean global O_3 production and loss rates computed in the model, as well as the lifetime of methylchloroform (CH_3CCl_3) against oxidation by tropospheric OH. The latter is a standard index of the global mean tropospheric OH concentration [*Spivakovsky et al.*, 2000]. The photochemical effects of aerosols beyond N_2O_5 hydrolysis reduce global O_3 production and loss by 6% and 7%, respectively. The global O_3 burden is unchanged

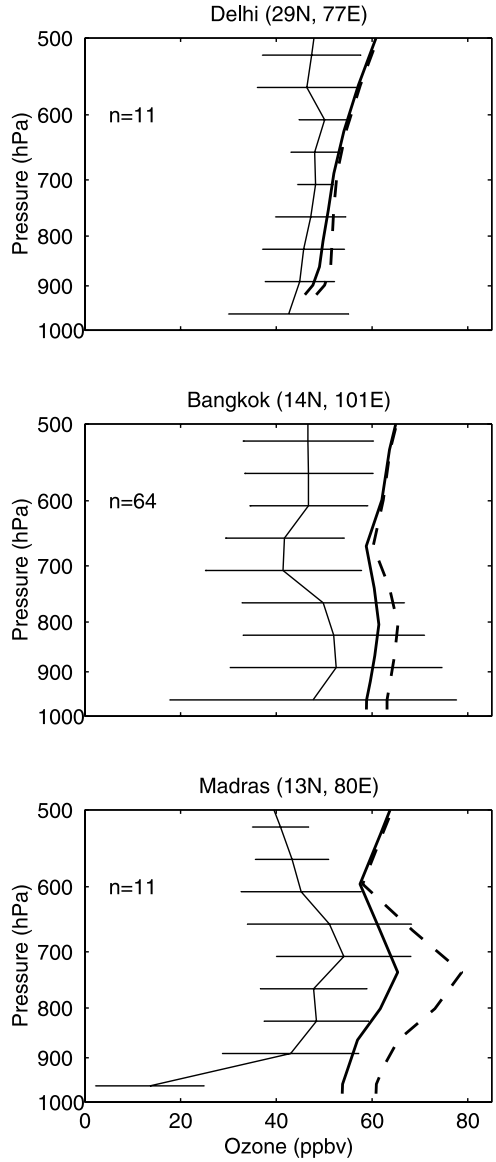

Figure 9. Comparison of observed and simulated O_3 concentrations over South Asia during March. Lines with error bars are aircraft measurements from MOZAIC, 1995–1999 [*Marenco et al.*, 1998]. Error bars indicate standard deviations. The number of observations is denoted by "n." The thick solid line is the monthly mean O_3 concentration from the standard simulation. The dashed line represents values from a simulation without the radiative effects or uptake of HO_2, NO_2, and NO_3 by aerosols.

because the large regional decreases in boundary layer O_3 are compensated by small increases throughout the tropical troposphere. The global O_3 production and loss rates calculated here are still at the high end of the current generation of global 3-D models, an issue discussed by *Bey et al.* [2001a]. Other models, including an earlier generation of our model [*Wang et al.*, 1998], indicate global production rates in the range 3300–4550 Tg yr^{-1} and global chemical loss rates in the range 2500–4100 yr^{-1} [*World Meteorological Organization*, 1998; *Lelieveld and Dentener*, 2000]. Our higher values relative to *Wang et al.* [1998] reflect more accurate treatment of radiative transfer through clouds [*Wild et al.*, 2000], as discussed by *Bey et al.* [2001a].

[31] *Dentener and Crutzen* [1993] previously found that N_2O_5 hydrolysis decreases the global mean tropospheric OH concentration (as measured by the lifetime of CH_3CCl_3) by 9%. We find here that the additional photochemical effects of aerosols globally decrease OH by an additional 9%. The radiative effects of mineral dust explain 60% of this decrease. The OH decrease is much larger in the Northern Hemisphere (13%) than the Southern Hemisphere (4%). The resulting global CH_3CCl_3 lifetime of 5.6 years against oxidation by tropospheric OH is consistent with estimates from observations of 5.7 ± 0.7 years [*Spivakovsky et al.*, 2000] and 6.0 (+1.0, −0.7) years [*Prinn et al.*, 2001].

6. Conclusions

[32] We have evaluated the sensitivity of tropospheric OH, O_3, and O_3 precursors to aerosol effects not usually included in global models: (1) aerosol scattering and absorption of ultraviolet radiation and (2) reactive uptake of HO_2, NO_2, and NO_3. We used for this purpose a global 3-D model of tropospheric chemistry (GEOS-CHEM) with specified global 3-D fields of sulfate, black carbon, organic carbon, sea salt, and mineral dust aerosol concentrations from a global model (GOCART) driven by the same meteorological fields. We did not examine the role of N_2O_5 hydrolysis in aerosols, whose importance is well established [*Dentener and Crutzen*, 1993] and which is included in all current-generation tropospheric chemistry models.

[33] We find important aerosol effects from reduction in photolysis frequencies and reactive uptake of HO_2 ($\gamma = 0.2$). Perturbations to photolysis frequencies are largely from absorbing aerosols; sulfate has little effect. Aerosols decrease the $O_3 \rightarrow O(^1D)$ photolysis frequency, $J(O(^1D))$, at the surface by 5–15% throughout most of the Northern Hemisphere, largely due to mineral dust, and by a factor of 2 in biomass burning regions, largely due to black carbon.

[34] Uptake of HO_2 by aerosols accounts for more than 10% of total HO_x ($\equiv$ OH + peroxy) loss in the boundary layer of most continental regions. The heterogeneous chemical effects of aerosols are largest where high concentrations

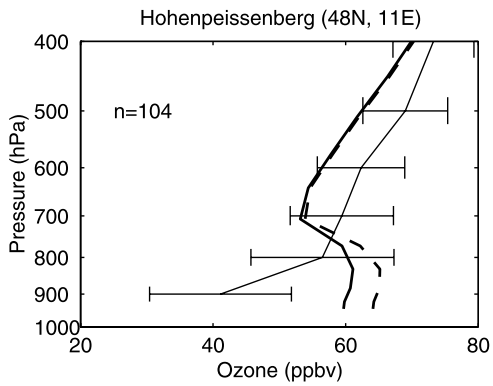

Figure 10. As in Figure 9, but for August at Hohenpeissenberg (48°N, 11°E, 975 m altitude). Measurements are from a 1980–1993 ozonesonde climatology [*Logan*, 1999].

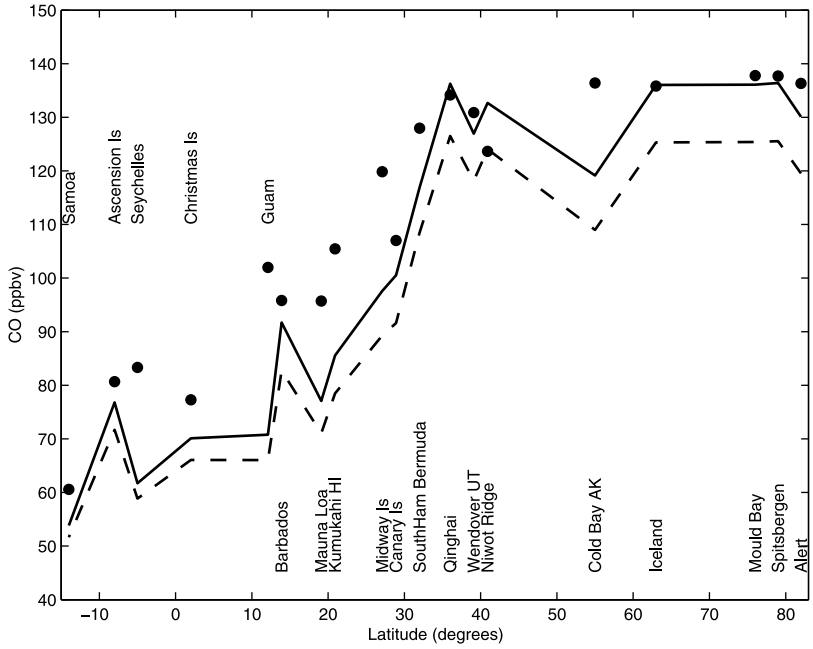

Figure 11. Comparison of observed and simulated annual mean CO concentrations in surface air for remote sites (annual mean concentrations less than 140 ppbv) of the Northern Hemisphere. Solid circles are observed values for 1988–1996 from *Novelli et al.* [1998]. Solid line is values from the simulation with full aerosol photochemistry. Dashed line is values from a simulation without the radiative effect of aerosols and without uptake of HO_2, NO_2, and NO_3 by aerosols.

of fine aerosols enable efficient gas-particle mass transfer. Uptake of HO_2 on aerosols accounts for up to 50–70% of HO_x loss over polluted regions of Eastern Europe (largely due to sulfate and organic carbon), and more than 70% over biomass burning areas of the tropics (largely due to organic carbon). Aerosols decrease boundary layer OH concentrations by 5–35% in most of the Northern Hemisphere, by a factor of 2 over northern Europe during August, and up to a factor of 4 over India during March.

[35] Reactive uptake of NO_2 ($\gamma = 10^{-4}$) and NO_3 ($\gamma = 10^{-3}$) have relatively small effects. These processes account for more than 10% of HNO_3 production only over the tropical North Atlantic, the Sahara, and the southern oceans. Over continental regions, the net effect of the aerosol processes considered here is to slightly increase NO_x due to OH depletion.

Table 4. Global Tropospheric O_3 Budget and CH_3CCl_3 Lifetime[a]

	Full Aerosol Photochemistry	N_2O_5 Hydrolysis Only[b]
Chemical production, Tg O_3 yr^{-1}	4924	5263
Chemical loss, Tg O_3 yr^{-1}	4377	4693
Burden, Tg O_3	322	323
Global CH_3CCl_3 lifetime, yr	5.6	5.2
NH CH_3CCl_3 lifetime, yr	5.4	4.8
SH CH_3CCl_3 lifetime, yr	5.8	5.6

[a]The production, loss, and burden of O_3 are actually for the extended odd oxygen family defined as $O_3 + NO_2 + 2 * NO_3$ + peroxyacylnitrates + $HNO_3 + 3 * N_2O_5$. They are calculated for the column extending up to the local model tropopause. The CH_3CCl_3 lifetime is calculated as the ratio of the total burden of atmospheric CH_3CCl_3 to the tropospheric loss rate against oxidation by OH [*Spivakovsky et al.*, 2000]. Values are annual means for September 1996 to August 1997 from the GEOS-CHEM model.

[b]This is the same as full aerosol photochemistry simulation but without radiative effects or uptake of NO_2, NO_3, and HO_2 by aerosols.

[36] We examined the implications of the above aerosol effects on the global model budgets of OH, O_3, and CO. Annual mean OH concentrations decrease by 9% globally (comparable to the effect of N_2O_5 hydrolysis) and by 13% in the Northern Hemisphere. About 60% of the global decrease is due to the radiative effects of mineral dust. The resulting CH_3CCl_3 lifetime against oxidation by tropospheric OH (5.6 years) is in better agreement with estimates constrained by observations. Annual mean global O_3 chemical production decreases by 6%, but the tropospheric O_3 burden remains unchanged. Concentrations of CO increase by 5–15 ppbv in most the Northern Hemisphere, improving agreement with observations at remote sites. Boundary layer O_3 decreases by 15–45 ppbv over South Asia during the biomass burning season in March, improving the comparison to aircraft observations (MOZAIC) although the model is still too high. Summertime boundary layer O_3 is reduced by 5–9 ppbv over northern Europe, and by 1–3 ppbv over the United States, again improving the model simulation with respect to observations over both regions. We conclude that surface O_3 concentrations over Europe and other industrial regions will increase if emissions of aerosols are reduced without corresponding reductions in O_3 precursors.

[37] **Acknowledgments.** Discussions with Mathew Evans, Bryan Duncan, Isabelle Bey, and Jennifer Logan were helpful. We thank Brendan Field and Arlene Fiore for contributions to model development. This work was supported by the NASA Atmospheric Chemistry Modeling and Analysis Program (ACMAP) and by a National Defense and Engineering Graduate Fellowship for Randall Martin.

References

Anderson, B. E., W. B. Grant, G. L. Gregory, E. V. Browell, J. E. Collins, G. W. Sachse, D. R. Bagwell, C. H. Hudgins, B. R. Blake, and N. J. Blake, Aerosols from biomass burning over the tropical South Atlantic

region: Distributions and impacts, *J. Geophys. Res.*, *101*, 24,117–24,137, 1996.

Bergamaschi, P., R. Hein, M. Heimann, and P. J. Crutzen, Inverse modeling of the global CO cycle, 1, Inversion of CO mixing ratios, *J. Geophys. Res.*, *105*, 1909–1927, 2000.

Bergamaschi, P., D. C. Lowe, M. R. Manning, R. Moss, T. Bromley, and T. S. Clarkson, Transects of atmospheric CO, CH_4, and their isotopic composition across the Pacific: Shipboard measurements and validation of inverse models, *J. Geophys. Res.*, *106*, 7993–8011, 2001.

Bey, I., D. J. Jacob, R. M. Yantosca, J. A. Logan, B. D. Field, A. M. Fiore, Q. Li, H. Y. Liu, L. J. Mickley, and M. G. Schultz, Global modeling of tropospheric chemistry with assimilated meteorology: Model description and evaluation, *J. Geophys. Res.*, *106*, 23,073–23,096, 2001a.

Bey, I., D. J. Jacob, J. A. Logan, and R. M. Yantosca, Asian chemical outflow to the Pacific: Origins, pathways and budgets, *J. Geophys. Res.*, *106*, 23,097–23,114, 2001b.

Chandra, S., J. R. Ziemke, P. K. Bhartia, and R. V. Martin, Tropical tropospheric ozone: Implications for dynamics and biomass burning, *J. Geophys. Res.*, *107*, 4188, doi:10.1029/2001JD000447, 2002.

Chin, M., R. B. Rood, S.-J. Lin, J. F. Muller, and A. M. Thompson, Atmospheric sulfur cycle simulated in the global model GOCART: Model description and global properties, *J. Geophys. Res.*, *105*, 24,671–24,687, 2000a.

Chin, M., D. Savoie, B. J. Huebert, A. R. Bandy, D. C. Thornton, T. S. Bates, P. K. Quinn, E. S. Saltsman, and W. J. De Bruyn, Atmospheric sulfur cycle in the global model GOCART: Comparison with field observations and regional budgets, *J. Geophys. Res.*, *105*, 24,689–24,712, 2000b.

Chin, M., P. Ginoux, S. Kinne, O. Torres, B. Holben, B. N. Duncan, R. V. Martin, J. A. Logan, A. Higurashi, and T. Nakajima, Tropospheric aerosol optical thickness from the GOCART model and comparisons with satellite and sunphotometer measurements, *J. Atmos. Sci.*, *59*, 461–483, 2002.

Chowdhury, Z., L. S. Hughes, L. G. Salmon, and G. R. Cass, Atmospheric particle size and composition measurements to support light extinction calculations over the Indian Ocean, *J. Geophys. Res.*, *106*, 28,597–28,606, 2001.

Chuang, C. C., J. E. Penner, K. E. Grant, J. M. Prospero, G. H. Rau, and K. Kawamoto, Cloud susceptibility and the first aerosol indirect forcing: Sensitivity to black carbon and aerosol concentrations, *J. Geophys. Res.*, *107*, 4564, doi:10.1029/2000JD000215, 2002.

Cooke, W. F., C. Liousse, H. Cachier, and J. Feichter, Construction of a $1° \times 1°$ fossil fuel emission data set for carbonaceous aerosol and implementation and radiative impact in the ECHAM4 model, *J. Geophys. Res.*, *104*, 22,137–22,162, 1999.

Dentener, F. J., Heterogeneous chemistry in the troposphere, Ph.D. thesis, Univ. of Utrecht, Utrecht, Netherlands, 1993.

Dentener, F. J., and P. J. Crutzen, Reaction of N_2O_5 on tropospheric aerosols: Impact on the global distributions of NO_x O_3, and OH, *J. Geophys. Res.*, *98*, 7149–7163, 1993.

Dentener, F. J., G. R. Carmichael, Y. Zhang, J. Lelieveld, and P. J. Crutzen, Role of mineral aerosol as a reactive surface in the global troposphere, *J. Geophys. Res.*, *101*, 22,869–22,889, 1996.

de Reus, M., F. Dentener, A. Thomas, S. Borrmann, J. Ström, and J. Lelieveld, Airborne observations of dust aerosol over the North Atlantic Ocean during ACE 2: Indications for heterogeneous ozone destruction, *J. Geophys. Res.*, *105*, 15,263–15,275, 2000.

de Rooij, W. A., and C. C. A. H. van der Stap, Expansion of Mie scattering matrices in generalized spherical functions, *Astron. Astrophys.*, *131*, 237–248, 1984.

Dickerson, R. R., S. Kondragunta, G. Stenchikov, K. L. Civerolo, B. G. Doddridge, and B. N. Holben, The impact of aerosols on solar ultraviolet radiation and photochemical smog, *Science*, *278*, 827–830, 1997.

Dickerson, R. R., M. O. Andreae, T. Campos, O. L. Mayol-Bracero, C. Neusuess, and D. G. Streets, Analysis of black carbon and carbon monoxide observed over the Indian Ocean: Implications for emissions and photochemistry, *J. Geophys. Res.*, *107*, 8017, doi:10.1029/2001JD000501, 2002.

Duncan, B. N., R. V. Martin, A. C. Staudt, R. M. Yevich, and J. A. Logan, Interannual and seasonal variability of biomass burning emissions constrained by remote-sensed observations, *J. Geophys. Res*, doi:10.1029/2002JD002378, in press, 2003.

Fiore, A. M., D. J. Jacob, I. Bey, R. M. Yantosca, B. D. Field, and J. G. Wilkinson, Background ozone over the United States in summer: Origin and contribution to pollution episodes, *J. Geophys. Res.*, *107*, 4275, doi:10.1029/2001JD000982, 2002.

Frost, G. L., et al., Photochemical ozone production in the rural southeastern United States during the 1990 Rural Oxidants in the Southern Environment (ROSE) program, *J. Geophys. Res.*, *103*, 22,491–22,508, 1998.

Ghan, S., N. Laulainen, R. Easter, R. Wagener, S. Nemesure, E. Chapman, Y. Zhang, and R. Leung, Evaluation of aerosol direct radiative forcing in MIRAGE, *J. Geophys. Res.*, *106*, 5295–5316, 2001.

Ginoux, P., M. Chin, I. Tegen, J. M. Prospero, B. Holben, O. Dubovik, and S. Lin, Sources and distributions of dust aerosols simulated with the GOCART model, *J. Geophys. Res.*, *106*, 22,055–22,074, 2001.

Gong, S., L. A. Barrie, and J.-P. Blanchet, Modeling sea-salt aerosols in the atmosphere, 1 Model development, *J. Geophys. Res.*, *102*, 3805–3818, 1997.

Grassian, V. H., Heterogeneous uptake and reaction of nitrogen oxides and volatile organic compounds on the surface of atmospheric particles including oxides, carbonates, soot and mineral dust: Implications for the chemical balance of the troposphere, *Int. Rev. Phys. Chem.*, *20*, 467–548, 2001.

Hansen, J. E., and L. D. Travis, Light scattering in planetary atmospheres, *Space Sci. Rev.*, *16*, 527–610, 1974.

Hauglustaine, D. A., G. P. Brasseur, P. J. Rasch, J.-F. Müller, L. K. Emmons, and M. A. Carroll, MOZART, a global chemical transport model for ozone and related chemical tracers, 2 Model results and evaluation, *J. Geophys. Res.*, *103*, 28,291–28,335, 1998.

He, S., and G. R. Carmichael, Sensitivity of photolysis rates and ozone production in the troposphere to aerosol properties, *J. Geophys. Res.*, *104*, 26,307–26,324, 1999.

Heikes, B. G., and A. M. Thompson, Effects of heterogeneous processes on NO_3, HONO, and HNO_3 chemistry in the troposphere, *J. Geophys. Res.*, *88*, 10,883–10,895, 1983.

Holben, B. N., et al., An emerging ground-based aerosol climatology: Aerosol optical depth from AERONET, *J. Geophys. Res.*, *106*, 12,067–12,097, 2001.

Jacob, D. J., Heterogeneous chemistry and tropospheric ozone, *Atmos. Environ.*, *34*, 2131–2159, 2000.

Jacob, D. J., B. D. Field, E. Jin, I. Bey, Q. Li, J. A. Logan, and R. M. Yantosca, Atmospheric budget of acetone, *J. Geophys. Res.*, *107*, 4100, doi:10.1029/2001JD000694, 2002.

Jacobson, M. Z., Isolating nitrated and aromatic aerosols and nitrated aromatic gases as sources of ultraviolet light absorption, *J. Geophys. Res.*, *104*, 3527–3542, 1999.

Jacobson, M. Z., A physically-based treatment of elemental carbon optics: Implications for global direct forcing of aerosols, *Geophys. Res. Lett.*, *27*, 217–220, 2000.

Jacobson, M. Z., and R. P. Turco, SMVGEAR: A sparse-matrix, vectorized Gear code for atmospheric models, *Atmos. Environ.*, *28*, 273–284, 1994.

Jaeglé, L., D. J. Jacob, W. H. Brune, and P. O. Wennberg, Chemistry of HO_x radicals in the upper troposphere, *Atmos. Environ.*, *35*, 469–489, 2001.

Köpke, P., M. Hess, I. Schult, and E. P. Shettle, Global aerosol data set, report, Max-Planck Inst. für Meteorol., Hamburg, Germany, 1997.

Kuhlbusch, T. A. J., M. O. Andreae, H. Cachier, J. G. Goldammer, J.-P. Lacaux, R. Shea, and P. J. Crutzen, Black carbon formation by savanna fires: Measurements and implications for the global carbon cycle, *J. Geophys. Res.*, *101*, 23,651–23,665, 1996.

Lal, S., and M. G. Lawrence, Elevated mixing ratios of surface ozone over the Arabian Sea, *Geophys. Res. Lett.*, *28*, 1487–1490, 2001.

Lawrence, M. G., P. J. Crutzen, P. J. Rasch, B. E. Eaton, and N. M. Mahowald, A model for studies of tropospheric photochemistry: Description, global distributions, and evaluation, *J. Geophys. Res.*, *104*, 26,245–26,277, 1999.

Lelieveld, J., and F. J. Dentener, What controls tropospheric ozone?, *J. Geophys. Res.*, *105*, 3531–3551, 2000.

Lelieveld, J., et al., The Indian Ocean Experiment: Widespread air pollution from South and Southeast Asia, *Science*, *291*, 1031–1035, 2001.

Leon, J. F., et al., Large-scale advection of continental aerosols during INDOEX, *J. Geophys. Res.*, *106*, 28,427–28,439, 2001.

Li, Q., et al., A tropospheric ozone maximum over the Middle East, *Geophys. Res. Lett.*, *28*, 3235–3238, 2001.

Li, Q., et al., Transatlantic transport of pollution and its effect on surface ozone in Europe and North America, *J. Geophys. Res.*, *107*, 4166, doi:10.1029/2001JD001422, 2002a.

Li, Q., D. J. Jacob, T. D. Fairlie, H. Liu, R. M. Yantosca, and R. V. Martin, Stratospheric versus pollution influences on ozone at Bermuda: Reconciling past analyses, *J. Geophys. Res.*, *107*, 4611, doi:10.1029/2002JD002138, 2002b.

Liang, J., and D. J. Jacob, Effect of aqueous-phase cloud chemistry on tropospheric ozone, *J. Geophys. Res.*, *102*, 5993–6001, 1997.

Liao, H., Y. L. Yung, and J. H. Seinfeld, Effects of aerosols on tropospheric photolysis rates in clear and cloudy atmospheres, *J. Geophys. Res.*, *104*, 23,697–23,707, 1999.

Liao, H., P. J. Adams, J. H. Seinfeld, L. J. Mickley, and D. J. Jacob, Interactions between tropospheric chemistry and aerosols in a unified GCM simulation, *J. Geophys. Res.*, *108*, 4001, doi:10.1029/2001JD001260, 2003.

Li-Jones, X., H. B. Maring, and J. M. Prospero, Effect of relative humidity on light scattering by mineral dust aerosol as measured in the marine boundary layer over the tropical Atlantic Ocean, *J. Geophys. Res.*, *103*, 31,113–31,121, 1998.

Liu, H., D. J. Jacob, L. Y. Chan, S. J. Oltmans, I. Bey, R. M. Yantosca, J. M. Harris, B. N. Duncan, and R. V. Martin, Sources of tropospheric ozone along the Asian Pacific Rim: An analysis of ozonesonde observations, *J. Geophys. Res.*, *108*, 4573, doi:10.1029/2001JD002005, 2003.

Logan, J. A., An analysis of ozonesonde data for the troposphere: Recommendations for testing 3-D models and development of a gridded climatology for tropospheric ozone, *J. Geophys. Res.*, *104*, 16,115–16,149, 1999.

Marenco, A., et al., Measurement of ozone and water vapor by Airbus in-service aircraft: The MOZAIC airborne program, An overview, *J. Geophys. Res.*, *103*, 25,631–25,642, 1998.

Martin, R. V., et al., An improved retrieval of tropospheric nitrogen dioxide from GOME, *J. Geophys. Res.*, *107*, 4437, doi:10.1029/2001JD001027, 2002a.

Martin, R. V., D. J. Jacob, J. A. Logan, I. Bey, R. M. Yantosca, A. C. Staudt, Q. Li, A. M. Fiore, B. N. Duncan, H. Liu, P. Ginoux, and V. Thouret, Interpretation of TOMS observations of tropical tropospheric ozone with a global model and in situ observations, *J. Geophys. Res.*, *107*, 4351, doi:10.1029/2001JD001480, 2002b.

Martin, S. T., Phase transitions of aqueous atmospheric particles, *Chem. Rev.*, *100*, 3403–3453, 2000.

Michel, A. E., C. R. Usher, and V. H. Grassian, Heterogeneous and catalytic uptake of ozone on mineral oxides and dusts: A Knudsen cell investigation, *Geophys. Res. Lett.*, *29*, 1665, doi:10.1029/2002GL014896, 2002.

Mishchenko, M. I., J. M. Dlugach, E. G. Yanovitskij, and N. T. Zakharova, Bidirectional reflectance of flat optically thick particulate layers: An efficient radiative transfer solution and applications to snow and soil surfaces, *J. Quant. Spectrosc. Radiat. Transfer*, *63*, 409–432, 1999.

Moise, T., and Y. Rudich, Reactive uptake of ozone by proxies for organic aerosols: Surface versus bulk processes, *J. Geophys. Res.*, *105*, 14,667–14,676, 2000.

Novelli, P. C., K. A. Masarie, and P. M. Lang, Distributions and recent changes in carbon monoxide in the lower troposphere, *J. Geophys. Res.*, *103*, 19,015–19,033, 1998.

Palmer, P. I., D. J. Jacob, K. Chance, R. V. Martin, R. J. D. Spurr, T. P. Kurosu, I. Bey, R. Yantosca, A. Fiore, and Q. Li, Air mass factor formulation for spectroscopic measurements from satellites: Application to formaldehyde retrievals from the Global Ozone Monitoring Experiment, *J. Geophys. Res.*, *106*, 14,539–14,550, 2001.

Palmer, P. I., D. J. Jacob, A. M. Fiore, R. V. Martin, K. Chance, and T. P. Kurosu, Mapping isoprene emissions over North America using formaldehyde column observations from space, *J. Geophys. Res*, doi:10.1029/2002JD002153, in press, 2003.

Patterson, E. M., D. A. Gillette, and B. H. Stockton, Complex index of refraction between 300 and 700 nm for Saharan aerosols, *J. Geophys. Res.*, *82*, 3153–3160, 1977.

Penner, J. E., et al., Aerosols, their direct and indirect effects, in *IPCC Third Assessment Report*, edited by J. T. Houghton et al., pp. 289–348, Cambridge Univ. Press, New York, 2001.

Phadnis, M. J., and G. R. Carmichael, Numerical investigation of the influence of mineral dust on the tropospheric chemistry of East Asia, *J. Atmos. Chem.*, *36*, 285–323, 2000.

Pósfai, M., J. R. Anderson, P. R. Buseck, and P. R. Sievering, Soot and sulfate aerosol particles in the remote marine troposphere, *J. Geophys. Res.*, *104*, 2213–2222, 1999.

Prinn, R. G., et al., Evidence for substantial variations of atmospheric hydroxyl radicals in the past two decades, *Science*, *292*, 1882–1888, 2001.

Ravishankara, A. R., Heterogeneous and multiphase chemistry in the troposphere, *Science*, *276*, 1058–1065, 1997.

Rhoads, K. P., P. Kelley, R. R. Dickerson, T. P. Carsey, M. Farmer, D. L. Savoie, and J. M. Prospero, Composition of the troposphere over the Indian Ocean during the monsoonal transition, *J. Geophys. Res.*, *102*, 18,981–18,995, 1997.

Schubert, S. D., R. B. Rood, and J. Pfaendtner, An assimilated data set for Earth Science applications, *Bull. Am. Meteorol. Soc.*, *74*, 2331–2342, 1993.

Sokolik, I., A. Andronova, and T. C. Johnson, Complex refractive index of atmospheric dust aerosols, *Atmos. Environ., Part A*, *27*, 2495–2502, 1993.

Spivakovsky, C. M., et al., Three-dimensional climatological distribution of tropospheric OH: Update and evaluation, *J. Geophys. Res.*, *105*, 8931–8980, 2000.

Takemura, T., H. Okamoto, Y. Maruyama, A. Numaguti, A. Higurashi, and T. Nakajima, Global three-dimensional simulation of aerosol optical thickness distribution of various origins, *J. Geophys. Res.*, *105*, 17,853–17,873, 2000.

Tegen, I., P. Hollrig, M. Chin, I. Fung, D. J. Jacob, and J. Penner, Contribution of different aerosol species to the global aerosol extinction optical thickness: Estimates from model results, *J. Geophys. Res.*, *102*, 23,895–23,915, 1997.

ten Brink, H. M., C. Kruisz, G. P. A. Kos, and A. Berner, Composition/size of the light-scattering aerosol in the Netherlands, *Atmos. Environ.*, *31*, 3955–3962, 1997.

Tie, X., G. Brasseur, L. Emmons, L. Horowitz, and D. Kinnison, Effects of aerosols on tropospheric oxidants: A global model study, *J. Geophys. Res.*, *106*, 22,931–22,964, 2001.

Torres, O., P. K. Bhartia, J. R. Herman, A. Sinyuk, P. Ginoux, and B. Holben, A long-term record of aerosol optical depth from TOMS observations and comparison to AERONET measurements, *J. Atmos. Sci.*, *59*, 398–413, 2002.

Tyndall, G. S., R. A. Cox, C. Granier, R. Lesclaux, G. K. Moortgat, M. J. Pilling, A. R. Ravishankara, and T. J. Wallington, Atmospheric chemistry of small organic peroxy radicals, *J. Geophys. Res.*, *106*, 12,157–12,182, 2001.

Wang, Y., D. J. Jacob, and J. A. Logan, Global simulation of tropospheric O_3-NO_x - hydrocarbon chemistry, 2, Model evaluation and global ozone budget, *J. Geophys. Res.*, *103*, 10,713–10,726, 1998.

Wild, O., X. Zhu, and M. J. Prather, Fast-J: Accurate simulation of in- and below-cloud photolysis in tropospheric chemistry models, *J. Atmos. Chem.*, *37*, 245–282, 2000.

World Meteorological Organization, Scientific assessment of ozone depletion, report, Global Ozone Obs. Syst., Geneva, 1998.

Zhang, Y., and G. R. Carmichael, The role of mineral aerosol in tropospheric chemistry in East Asia - A model study, *J. Appl. Meteorol.*, *38*, 353–366, 1999.

Zhang, Y., Y. Sunwoo, V. Kotamarthi, and G. R. Carmichael, Photochemical oxidant processes in the presence of dust: An evaluation of the impact of dust on particulate nitrate and ozone formation, *J. Appl. Meteorol.*, *33*, 813–824, 1994.

M. Chin and P. Ginoux, NASA Goddard Space Flight Center, Code 916, Greenbelt, MD 20771, USA. (chin@rondo.gsfc.nasa.gov; ginoux@rondo.gsfc.nasa.gov)

D. J. Jacob and R. M. Yantosca, Division of Engineering and Applied Sciences, Harvard University, G3D Pierce Hall, 20 Oxford Street, Cambridge, MA 02138, USA. (djj@io.harvard.edu; bmy@io.harvard.edu)

R. V. Martin, Harvard-Smithsonian Center for Astrophysics, 60 Garden Street, MS 50, Cambridge, MA 02138, USA. (rvmartin@fas.harvard.edu)

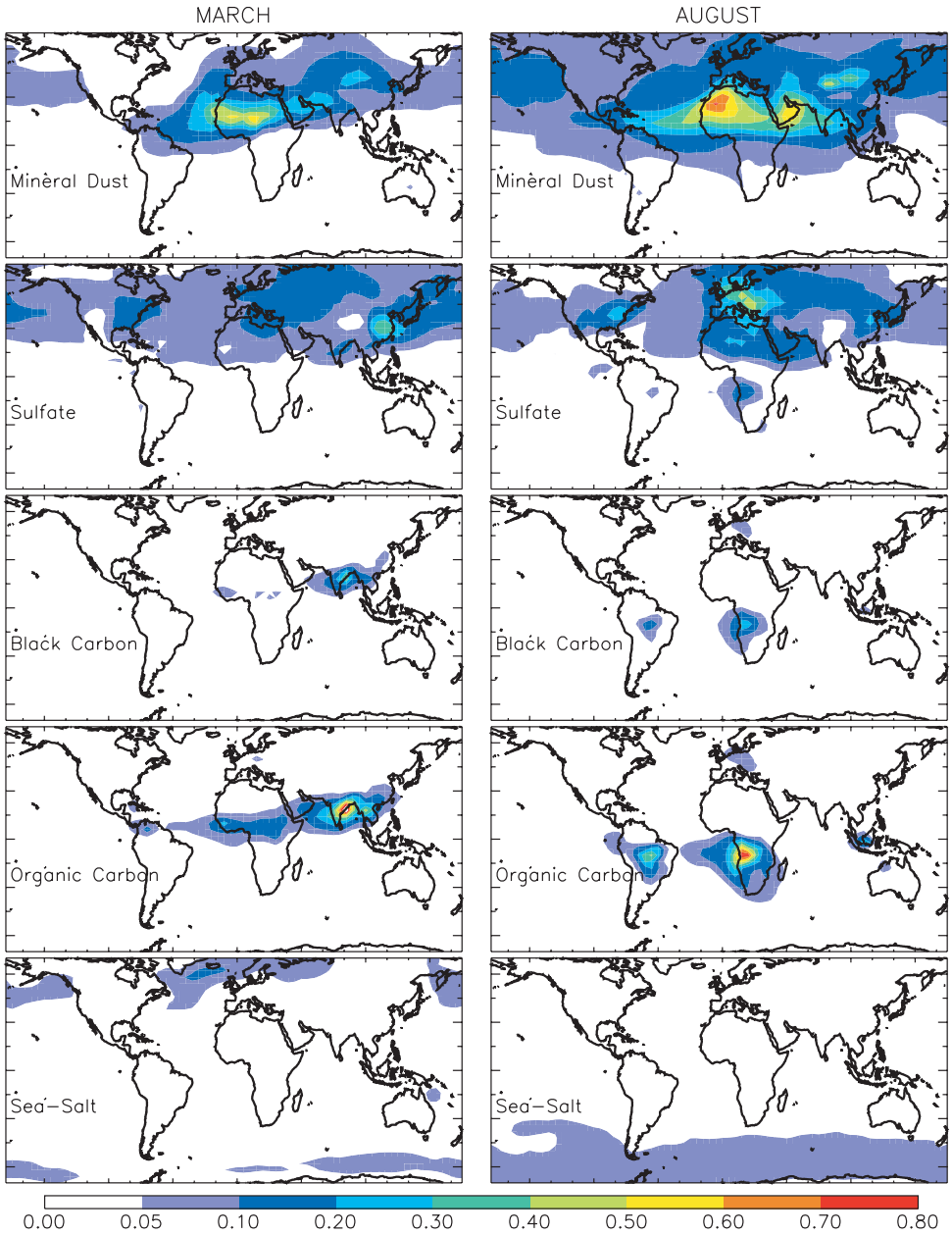

Figure 1. Modeled monthly mean optical depth at 400 nm of different aerosol types for March 1997 (left column) and August 1997 (right column). Values are calculated from mass concentration fields from *Ginoux et al.* [2001] for mineral dust and from *Chin et al.* [2002] for the other aerosol types.

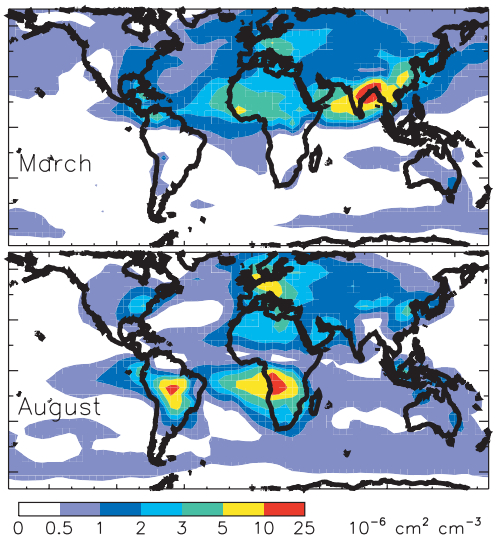

Figure 2. Modeled monthly mean total aerosol surface area in the lower troposphere (~600 m above the surface) for March and August 1997. Values are calculated from mass concentration fields from *Ginoux et al.* [2001] for mineral dust and from *Chin et al.* [2002] for the other aerosol types.

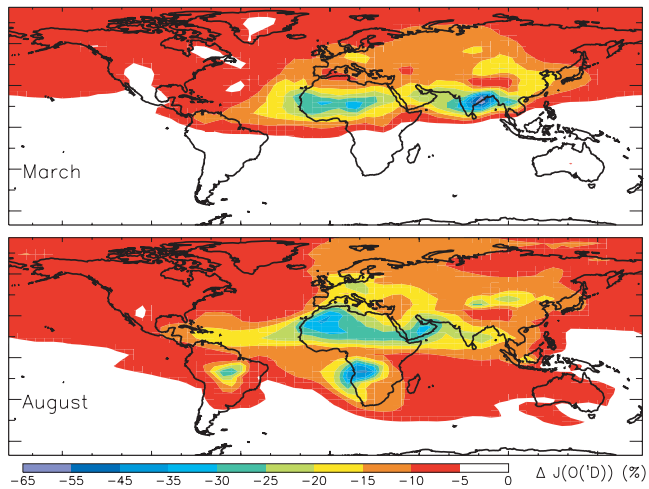

Figure 3. Sensitivity to aerosols of the $O_3 \rightarrow O(^1D)$ photolysis frequency ($J(O(^1D))$) in surface air. Values are monthly mean model results for March and August 1997.

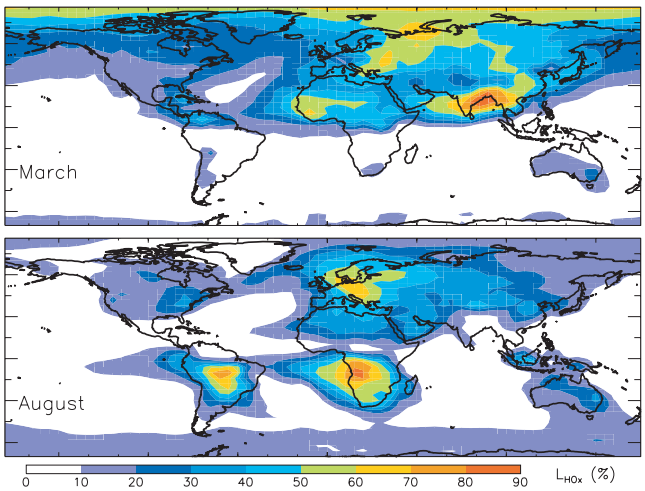

Figure 4. Fraction of total HO_x loss in the lower troposphere (~600 m above the surface) contributed by uptake of HO_2 by aerosols. Values are monthly mean model results for March and August 1997.

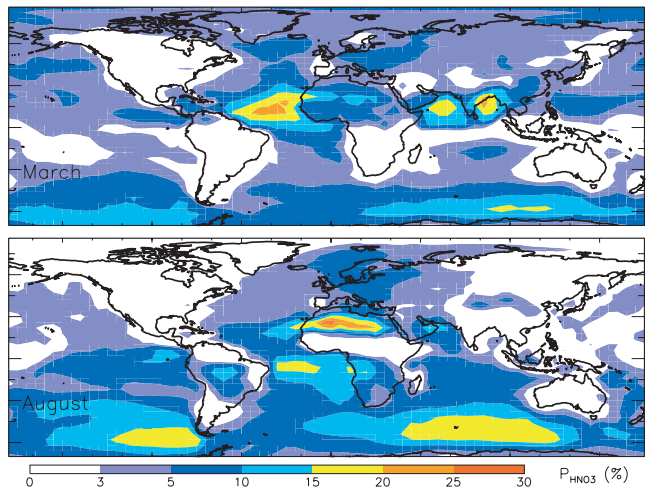

Figure 5. Fraction of total HNO_3 production in the lower troposphere (~600 m above the surface) contributed by uptake of NO_2 and NO_3 by aerosols. Values are monthly mean model results for March and August 1997.

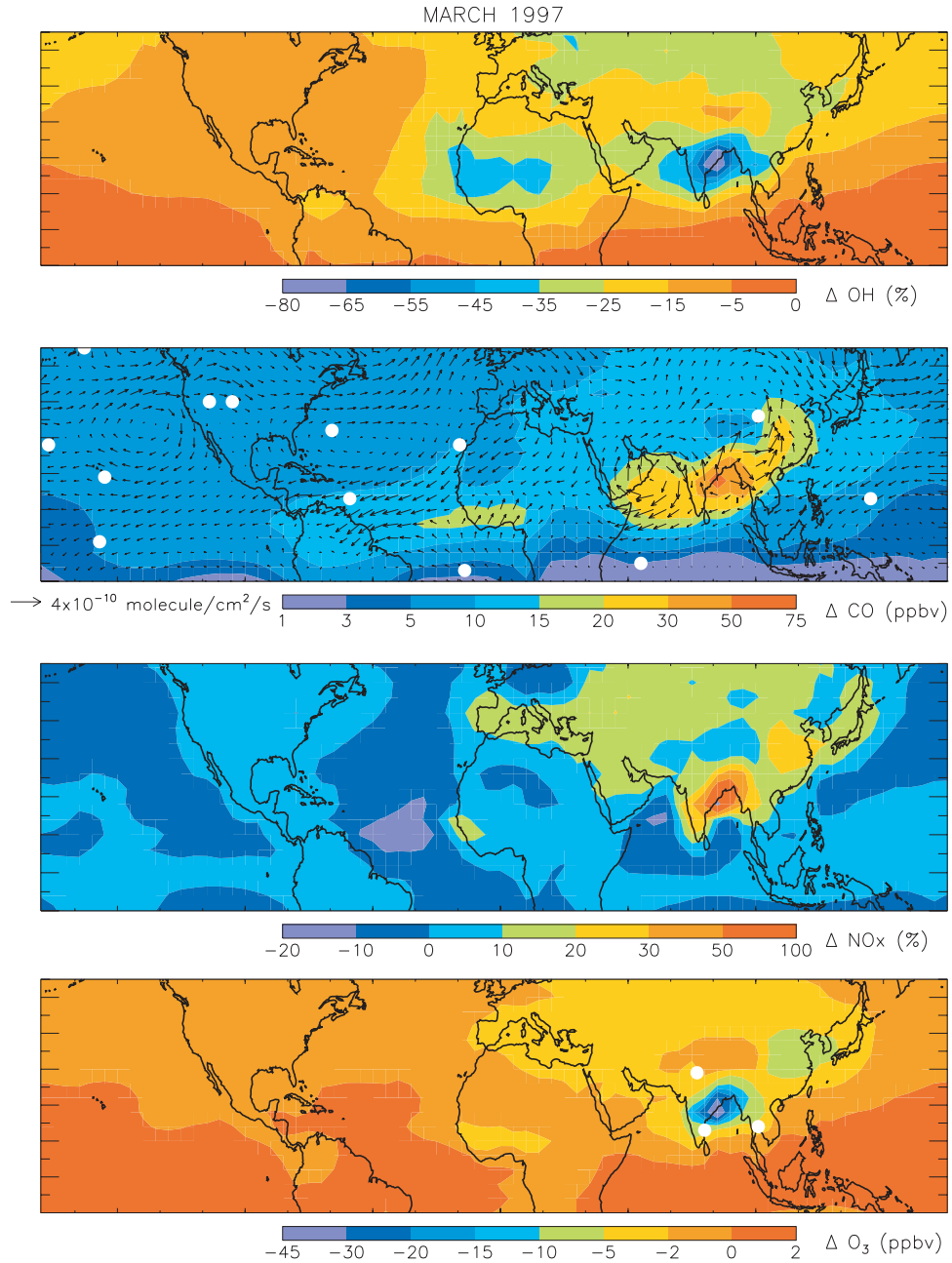

Figure 7. Changes in OH, CO, NO_x, and O_3 concentrations in the lower troposphere (~600 m above the surface) from scattering and absorption by aerosols, and from uptake of HO_2, NO_2, and NO_3 by aerosols, as determined by difference with a simulation that did not include these effects. Values are model monthly means during March. White circles show the locations of observations compared to the model in section 4. Also shown is the change in the CO flux due to the above aerosol effects.

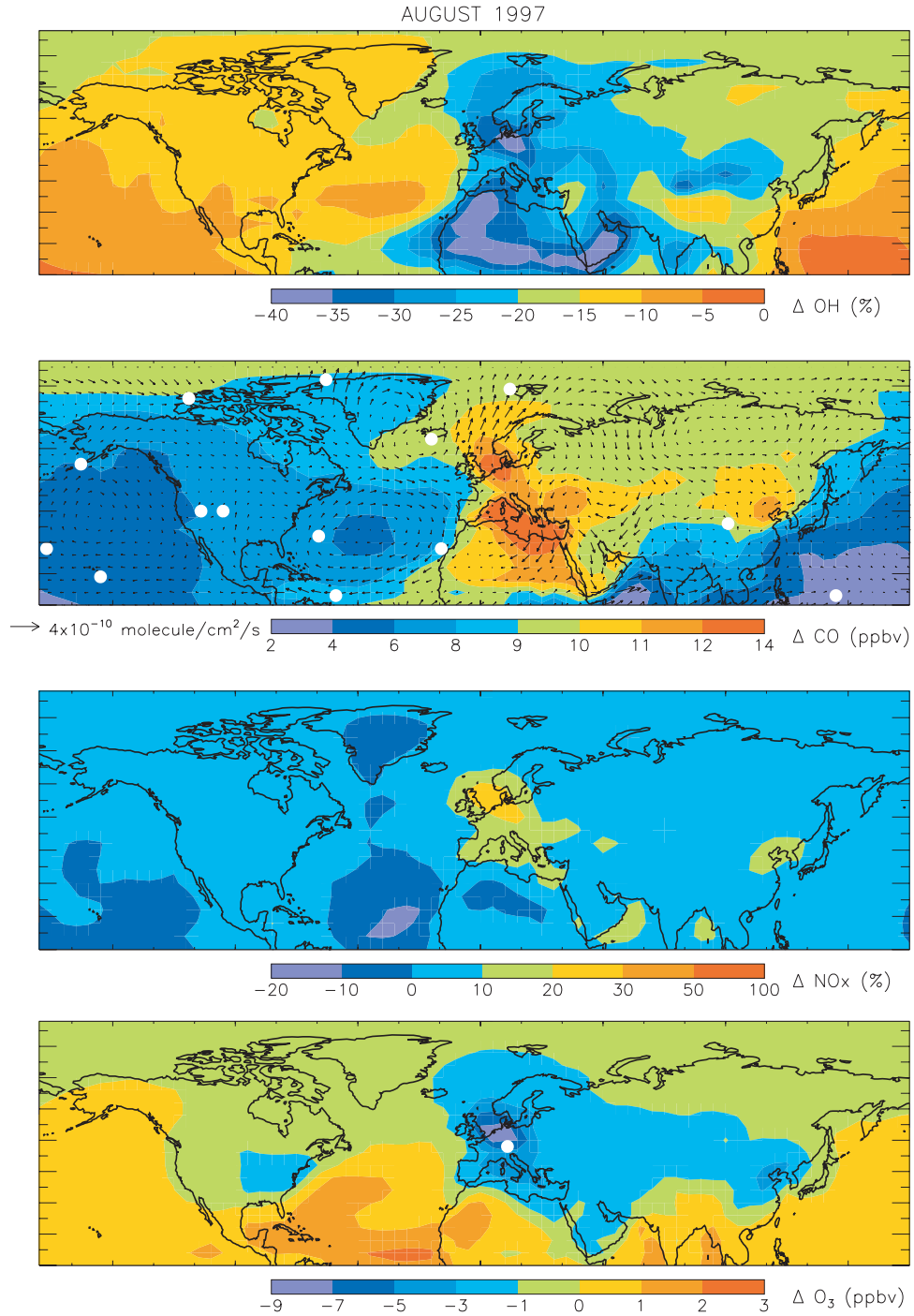

Figure 8. As in Figure 7, but for August.